Acid, Alkali, Chloride and Carbonation Resistance of Ternary Blended High Volume Mineral Admixed Concrete

B. B. Das[1*], Leon Black[2], Salim Barbhuiya[3], K Snehal[4] and E P Sumukh[5]

[1]Professor, Department of Civil Engineering, National Institute of Technology Karnataka, Surathkal, Karnataka, India, 575 025, E-Mail: bibhutibhusan@gmail.com

[2]Professor of Infrastructure Materials, School of Civil Engineering, University of Leeds, United Kingdom, Woodhouse, Leeds LS2 9JT, UK, E-Mail: L.Black@leeds.ac.uk

[3]Department of Engineering and Construction, University of East London, United Kingdom, University Way, London, E16 2RD, E-Mail: S.Barbhuiya@uel.ac.uk

[4]Former Research Scholar, Department of Civil Engineering, National Institute of Technology Karnataka, Surathkal, Karnataka, India, 575 025, E-Mail: snehalshine090@gmail.com

[5]Research Scholar, Sustainable Construction and Building Materials Laboratory, Department of Civil Engineering, National Institute of Technology Karnataka, Surathkal, Karnataka, India, 575 025, E-Mail: sumukhgowdaekkeri@gmail.com

*Corresponding Author

Abstract

The World Bank study predicts that 4°C warming will bring high temperatures, sea-level rise, and saltwater intrusion to India's southwest coast, damaging coastal concrete structures. Increased CO_2 from industrialization exacerbates this, necessitating durable, low-carbon concrete. Combined use of fly ash (FA) and ground granulated blast furnace slag (GGBFS) as high-volume OPC replacements boosts performance while reducing concrete's carbon footprint. In this perspective current study examines the durability of concrete against aggressive agents (H_2SO_4, $MgSO_4$, NaCl, and CO_2) causing premature deterioration of concrete structures along the southwest coast of India. Initially, three cost-effective sustainable concrete mix designs were developed, incorporating 50% replacement of OPC with locally available supplementary cementitious materials, specifically FA and GGBFS. These mixes were then evaluated for their mechanical and durability performances. The impact of aggressive ions (SO_4^{2-}, Cl^-, and CO_3^{2-}) was studied by examining the changes in mechanical performance and phase assemblages. Thermogravimetric analysis (TGA) and Fourier transform infrared spectroscopy (FTIR) techniques were used to estimate the phase compositions.

Ternary blended concrete having 50% OPC+ 30% GGBFS + 20% FA exhibited optimal synergistic performance, enhancing pozzolanic and hydraulic reactions for better resistance to harmful ions. The sorptivity test confirmed that as GGBFS content increased, the sorption rate decreased, indicating the higher reactive nature of GGBFS to that of FA. Deleterious compounds formed due to the action of SO_4^{2-}, Cl^-, and CO_3^{2-} were identified to be ettringite ($Ca_6Al_2(SO_4)3(OH)_{12}.32H_2O$, AFt) and gypsum ($CaSO_4.2H_2O$, Gy), Friedel's salt ($Ca_4Al_2(OH)_{12}Cl_2.4H_2O$, Fs) and polymorphs of calcium carbonate (CaCO3), respectively through TG mass loss curve. These results were corroborated by FTIR analysis, which showed predominant characteristic bands at 662 cm^{-1} for SO_4^{2-}, 459 cm^{-1} for Mg–O stretching, 790 cm^{-1} for Al–OH bending, and 1431-1443 cm^{-1} for C–O, confirming the presence of the deleterious compounds.

Keywords: Cement, Fly Ash, GGBFS, climate resilient concrete, ettringite, gypsum, Friedel's salt and calcium carbonate**.**

1. Introduction

Rapid urbanization and augmented challenges posed by climate change have driven the need for sustainable, and robust infrastructure. Ordinary Portland cement (OPC) which is responsible for about 8% of global anthropogenic CO_2 emissions, is the world's most popular construction material, yet has a high energy demand, consumes vast quantities of materials [1,2]. In light of this, fly ash and ground granulated blast furnace slag (GGBFS), are considered worthy components for manufacturing cement with lower Portland clinker contents thanks to their production volumes and physicochemical properties [3,4]. Global coal and steel industries produce around 1000 million tonnes and 330 million tonnes of fly ash and GGBFS, respectively per annum[5,6]. In addition to lowering demand for Portland cement clinker and so reducing CO_2 emissions, using fly ash and GGBFS in concrete offers a number of technical benefits, including increased durability [7,8].

Fly ash is an extensively studied and widely used supplementary cementitious material (SCM) in cementitious composites. Fly ash particles are spherical and generally cenospheres, whose average particle size lies close to that of cement particles [1,9,10]. The American standard categorizes fly ash as class C and class F depending on its oxide composition [11]. Class F fly ashes are pozzolanic and are considered to be more applicable for use in cementitious composites because of their lower calcium contents [12]. The glassy aluminosilicate component of fly ash particles reacts with calcium hydroxide (CH) to form calcium silicate hydrates [13], which helps to contribute to the long-term strength and durability of cementitious composites [10]. The pore-filling ability of fly ash particles also further refines the pore structure of cementitious composites, providing better resistance to the ingress of chemical ions [1]. The use of fly ash can also significantly improve concrete flow due to the ball-bearing action of the spherical particles [14]. Using fly ash also reduces heat evolution during hydration [13]. However, it is reported that at replacement levels above 20-30%, there can be a reduction in performance, depending on the quality of fly ash [15]. Furthermore, fly ash can extend the setting time and retard early strength gain [16].

GGBFS is another widely used SCM, produced by quenching of molten slag during iron production. It is a glassy aluminosilicate containing calcium and magnesium [7]. GGBFS possesses latent hydraulic properties due to its calcium content, with hydration resulting in C-S-H gel formation [17]. However, the hydration of GGBFS alone is very slow. Blending of GGBFS with cement increases the rate of hydration due to the pozzolanic reaction with

85 portlandite. Thus, GGBFS composite cements typically have calcium hydroxide contents
86 between those of OPC and OPC-FA blends [18]. GGBFS, with a particle size of approximately
87 40 μm, can replace 30-65% OPC [18,19]. The use of GGBFS in cement composites can lead
88 to improved workability, long-term strength, reduced water permeability, greater resistance to
89 sulphate/chloride ingress, and resistance to corrosion in reinforced concrete [20]. However,
90 blending cement with GGBFS can also prolong setting times and lead to lower early-age
91 strength [21].

92 Composite cements show improved resistance to steel reinforcement when exposed to
93 aggressive environments such as carbonation and chloride exposure [22,23] due to their
94 improved microstructures and phase assemblages [24,25]. More recently, there has been
95 growing interest in exploring the potentiality of ternary blended cementitious composites in
96 dealing with multiple aggressive phenomena [26–28]. The combined use of GGBFS and fly
97 ash in concrete offers an opportunity to harness the complementary qualities of both SCMs to
98 produce robust, low-carbon concrete. Synergetic action of GGBFS and fly ash would augment
99 the overall performance as well as improve the sustainability supporting the evolution on the
100 way to greener construction approaches. The effects of replacing high-volume ordinary
101 Portland cement (OPC) with fly ash and/or GGBFS on the binary and ternary blends' flow,
102 compressive strength, and environmental effects were examined in one such study. With the
103 addition of 20% to 30% fly ash, the study discovered that the usage of ternary mixes improved
104 the flow properties. The same mix reduced the early-age compressive strength, while an
105 improvement in the late-age strength was observed [29]. Chen et al. concluded that the presence
106 of a synergetic effect between fly ash and GGBFS improved the pozzolanic and hydraulic
107 activities with enhanced durability of recycled aggregate concrete [30].

108 To accomplish these, a proper mix design is crucial, coupled with the required quality control
109 procedures. Such research is limited, which necessitates a better understanding of the
110 microstructures, phase assemblages and durability performance of ternary FA-GGBFS-OPC
111 blends. In this regard, a better understanding of the changes caused by aggressive species will
112 aid predictions of concrete performance under future climate conditions. In this perspective,
113 the present study focuses on the combined utilization of locally available industrial mineral
114 admixtures, fly ash and GGBFS, as high-volume replacements for ordinary Portland cement
115 (OPC) to develop durable concrete for use in Indian coastal and marine structures. Three high-
116 volume (50%) replacement concrete mixes were designed, with different FA: GGBFS ratios,
117 i.e., 25% FA + 25% GGBFS; 20% FA + 30% GGBFS; 30% FA + 20% GGBFS. Further, the

mechanical performance of concretes was tested. This was followed by testing resistance to aggressive exposures such as acid (H_2SO_4), sulphate ($MgSO_4$), chloride (NaCl) and carbon dioxide (3.5% CO_2). Subsequently, the concretes exposed to aggressive media were characterized using thermogravimetric analysis (TGA) and Fourier transform infrared spectroscopy (FTIR).

2. Experimental investigation

2.1 Materials

Ordinary Portland cement (OPC) of 53 grade (i.e., OPC-53) conforming to Indian standard [31] was used in this study. Class F fly ash (FA) and GGBFS confirming to ASTM C 618 [11] and ASTM C 989 standards [18], respectively were used as a partial replacement of OPC. Locally available river sand conforming to zone-II according to Indian standard [32] and crushed coarse aggregates with a maximum size of 20 mm were used [33]. A high-performance polycarboxylic ether-based superplasticizer was used. The oxide compositions and physical properties of the binder materials are shown in Table 1. The physical properties of the aggregates are shown in Table 2, while Fig. 1a) presents the gradation curves of various raw materials used in the present study.

Table 1 Oxide composition and physical properties of OPC, FA and GGBFS

Chemical Properties		OPC	Fly ash	GGBFS
SiO_2		20.89	60.6	37.7
Al_2O_3		5.55	28.6	14.4
Fe_2O_3		4.98	3.9	1.1
CaO		60.46	1.7	37.3
MgO		1.27	1.8	8.7
SO_3		2.39	1.2	0.2
Na_2O		0.232	0.4	-
MnO		-	-	0.02
Insoluble residue		2.88	-	1.6
Glass content		-	-	92
K_2O		0.45	0.1	-
Loss on ignition (LOI)		2.26	1.6	1.4
Specific gravity		3.15	2.2	2.9
Fineness (m^2/kg)		300	265	382
Setting time (mins)	Initial	110	-	-
	Final	170	-	-

Table 2 Physical properties of aggregates

Sl. No	Property		Fine aggregates	Coarse aggregates
1	Specific gravity		2.56	2.63
	Bulk density	Loose	1436 kg/m^3	1333 kg/m^3

2		Compacted	1700 kg/m^3	1567 kg/m^3
3	% of voids		38.2	47.1
4	Moisture content		Nil	Nil
5	Water absorption		1%	0.5%
6	Fineness modulus		2.74	2.17
7	Flakiness index		-	12%
8	Elongation index		-	7%
9	Silt content		1.1%	-

2.2 Mix proportion

Three mixes of M30 grade, high-volume mineral admixture concretes (HVMAC) were designed with different proportions of FA and GGBFS as replacements for OPC. The total OPC replacement level was kept constant at 50%. Additionally, M30 grade control mix without any OPC replacement was used as a reference mix. A constant water-to-binder ratio of 0.44 was maintained throughout this study. Mix proportions are presented in Table 3.

Table 3 Mix proportion details of concrete mixes

M30 grade	Mix Designation	OPC (kg/m^3)	Fine Aggregate (kg/m^3)	Coarse Aggregate (kg/m^3)	FA (kg/m^3)	GGBFS (kg/m^3)	Water (ltr)
Control (100% OPC)	C	341	840.80	1127.78	-	-	150
25% FA + 25% GGBFS + 50% OPC	25F25G	187.5	812.21	1089.40	93.75	93.75	150
20% FA + 30% GGBFS + 50% OPC	20F30G	187.5	813.38	1090.00	75	112.5	150
30% FA + 20% GGBFS + 50% OPC	30F20G	187.5	808.80	1084.80	112.5	75	150

The rationale behind the selected proportions in the study (Table 3) was to achieve a 50% total replacement of Ordinary Portland Cement (OPC) with supplementary cementitious materials. These specific ratios were chosen to explore a range of potential benefits and to understand how different combinations of FA and GGBFS affect the concrete properties, such as mechanical strength, durability, and overall performance. The study aimed to balance the pozzolanic and hydraulic effects of materials and identify effective concrete blends. Although an orthogonal experimental design could provide a comprehensive analysis, the selected proportions were based on practical considerations and previous research insights [29,34].

2.3 Methodology

2.3.1 Sample preparation

Concrete mixes were prepared using a drum-type laboratory concrete mixer. Mixes were cast in 100 mm cube moulds, 100 × 100 × 500 mm prisms, and 50 mm diameter 300 mm long cylinders for conducting compressive, flexural and split tensile strength testing respectively. Further, 100 mm cubes with centrally-placed, vertically-reinforced 10 mm steel bar were cast for undertaking bond strength / pull-out strength tests (as shown in Fig. 1b)). Specimens were cast into respective moulds and vibrated using a vibrating table before being moist cured for 24 hours under laboratory conditions (27-32°C; 95% humidity). Specimens were demoulded and water-cured for predefined curing ages. Additional 100 mm cube specimens were cast to examine the sorptivity, acid resistance, alkali resistance, chloride resistance, and accelerated carbonation resistance of high-volume mineral admixture concrete.

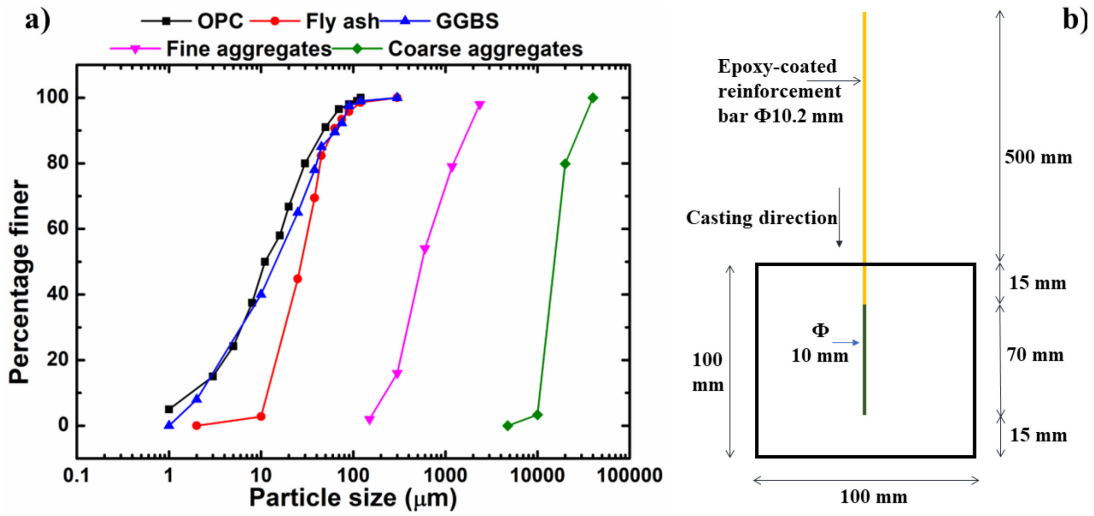

Fig. 1a) Particle size distribution curve of the raw materials used; **b)** Line diagram of the specimen cast for measuring the ultimate bond strength

2.3.2 Mechanical Properties

Compressive strength and flexural strength were determined according to Indian standard [35], using compressive and flexural strength testing machines capable of loading to 2000 kN and 200 kN at 140 kg/cm^2/minute and 180 kg/minute, respectively. Split tensile strength was assessed based on Indian standard [36] using a compression strength testing machine with a 2000 kN capacity and a loading rate of 2 kN per minute. To ensure a point load, billets were kept exactly in the mid of the horizontally placed cylindrical specimens.

Ultimate bond strength was determined using the aforementioned cube specimens containing a single reinforcement bar (deformed and Fe500). Bond strength test was conducted as per the Indian standard [37]. Universal testing machine was used for conducting bond strength test, with a load applied to the reinforcing bar at a rate not greater than 2.250 kg/min.

All tests were recorded in triplicate, with average values reported.

2.3.3 Durability properties

2.3.3.1 Sorptivity test

Concrete sorptivity was assessed by measuring the increase in weight of concrete cubes upon immersion in water as a function of time when only one surface of the specimen was exposed to water. Tests were conducted in triplicate as per American standards [38] after curing for 14 and 28 days. All samples were preconditioned by oven drying at 105°C for 24 hours before testing.

2.3.3.2 Aggressive exposure

All concrete mixes were water-cured for 14 and 28 days before exposure to aggressive solutions of acid (H_2SO_4), sulphate ($MgSO_4$), chloride (NaCl) and accelerated carbon dioxide. The different tests were as follows.

Acid [39], sulphate [40] and chloride [41] attack tests were conducted using 5% sulphuric acid (H_2SO_4, pH 0.3), 5 % magnesium sulphate ($MgSO_4$, pH 12) and 3.5% Sodium Chloride (NaCl, pH 7) prepared using normal tap water [39–41]. Concrete cubes were cured for 14 and 28 days before submersion in their respective aggressive solutions. Care was taken to maintain the specific pH levels for each solution throughout exposure. To maintain specific pH levels throughout the exposure period, the following procedures were, at first, specific pH levels were calibrated using pH meters with standard solutions, then accurate chemical concentrations were used for exposure solutions, and solutions were regularly monitored for pH during exposure. Adjustments were made with acid or base solutions as needed. Specimens exposed to 30-, 60-, and 365 days were then removed from the solutions and allowed to attain saturated surface dry, before being weighed and determining their compressive strength. Weight and strength loss were assessed with the initial values ($W_{\text{before exposure}}$ and $\rho_{\text{before exposure}}$) at each curing age (14 or 28 days) using Eq. 1 and 2, respectively.

$$Weight\ loss\ (\%) = \frac{W_{before\ exposure} - W_{after\ exposure}}{W_{before\ exposure}} \times 100 \quad (1)$$

$$Strength\ loss\ (\%) = \frac{\rho_{before\ exposure} - \rho_{after\ exposure}}{\rho_{before\ exposure}} \times 100 \quad (2)$$

To conduct the carbonation test [42], concrete cubes of 100 mm × 100 mm × 100 mm were cured for 14 or 28 days before being placed in the carbonation chamber under accelerated carbonation conditions. The set environment was well maintained inside the carbonation chamber at 3.5% CO_2, 70% relative humidity and 27±2°C temperature for an exposure period of 60 or 90 days. All the specimens were air dried in the ambient condition for 4 hrs before placing the specimens in the carbonation chamber to achieve saturated surface dry condition. At the end of exposure period, carbonation depth, change in weight and change in compressive strength were noted. Carbonation depths were determined by spraying freshly sliced concrete specimens with phenolphthalein solution [43]. Alkaline regions (pH >9) appear pink and carbonated regions appear colourless. The carbonation depth from the concrete surface was then determined using Vernier callipers with 0.01 mm accuracy and the measurement was conducted as per RILEM CPC-18 [44] on sliced specimens obtained from three cubes under every concrete mix. Further, the average value was reported.

2.3.4 Thermogravimetric analysis (TGA)

Crushed concrete samples exposed to all aggressive media were collected and crushed gently to < 75 µm. These powdered samples were analysed by thermogravimetric analysis (TGA) using RIGAKU TG-DTA 8112 analyser over the temperature range of 25-900 °C under nitrogen (purge rate: 20 ml/min, heating rate: 10 °C/min).

2.3.5 Fourier transform infrared spectroscopy (FTIR)

FTIR analysis was conducted on the aforementioned powdered concrete samples using a Bruker (Alpha II) instrument. Spectrums were recorded over the range of 4000 to 600 cm^{-1} with a resolution of 2 cm^{-1}.

3. Results and discussions

3.1 Compressive strength

Compressive strength results for all concrete mixes after 2, 7, 28, 56, and 90 days of curing are presented in Fig. 2 a). Fig. 2b) represents the percentage change in compressive strength the curing age of 90 days with respect to 28 days of curing.

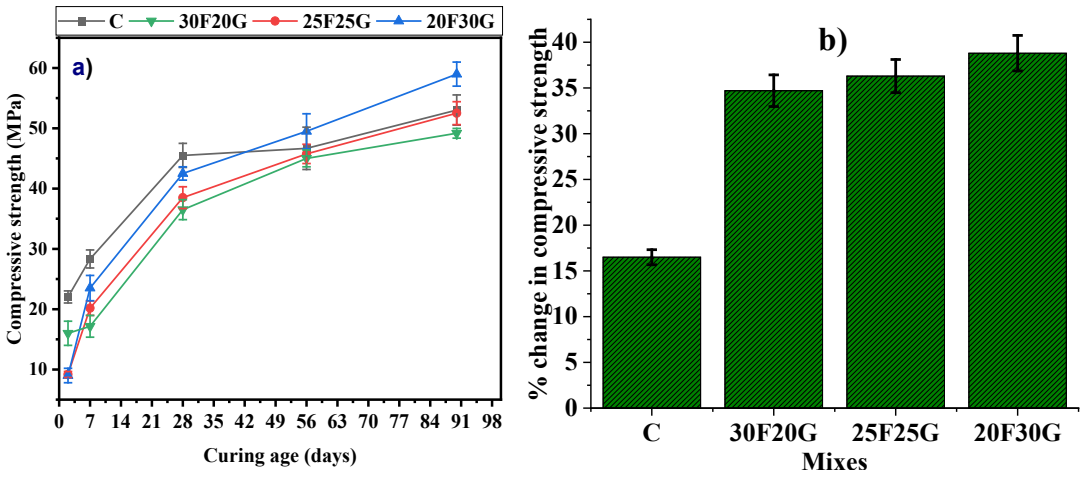

Fig. 2 a. Compressive strength development of control and HVMACs, **b.** percentage change in compressive strength at the curing age of 90 days with respect to 28 days of curing

Compressive strength development to 28 days was greatest for the control mix (C), with a compressive strength of 45.5 MPa. Strength gain was more gradual after that, such that the 28-day strength was 86% that of the 90-day compressive strength (53 MPa). This reflects the hydration and consumption of the anhydrous cement grains [45,46]. In the case of HVMAC mixes strength development was more gradual and all of the HVMAC mixes showed lower strengths than the control mixes up to 28 days. However, at later ages, strength development was seen to be more pronounced for HVMAC mixes (Fig. 2b). This is due to the dilution effect and the much slower rate of subsequent FA and GGBFS hydration [47]. The mix containing 30% GGBFS (20F30G) showed the highest strength amongst all HVMAC mixes.

3.2 Flexural strength

Figure 3a) shows the flexural strength results for all of the concrete mixes. As with compressive strength, flexural strength values for HVMAC mixes were typically lower than the control, and strength development was more gradual. Flexural strengths of mixes 25F25G, 20F30G, and 30F20G were reduced by 76%, 74% and 77%, respectively at 2 days and by 45%, 36% and 53%, respectively at 7 days compared to the control mix. As with compressive strength, the performance of the HVMAC mixes improved with increasing GGBFS content, such that the flexural strength of mix '20F30G' exceeded that of the control mix by 1%, 6% and 8% at 28, 56 and 90 days, respectively. FA is less reactive than GGBFS, particularly at an early age [48], and this is exacerbated by the increased fineness of the GGBFS used in this study [49].

3.3 Split tensile strength

Fig. 3b) shows the split tensile strength results for all concrete mixes. Again, all of the HVMAC mixes gained strength very slowly and were weaker than the control concrete to 28 days, particularly at early age. By 56 days the split tensile strengths of the blended mixes were comparable to that of control mix. Again, the strengths of the blended mixes correlated with the GGBFS content.

3.4 Bond strength

Figure 3c) shows the bond strength for each mix at 2, 7 and 28 days of curing. The bond strengths of all HVMAC mixes were lower than those of the control mix (C) at all ages, but particularly at early ages. However, by 28 days the two mixes with the highest GGBFS contents showed bond strengths comparable to the control. As with all of the other strength data, the difference between the HVMAC mixes and the control can be explained by a combination of clinker dilution and the slow pozzolanic reaction.

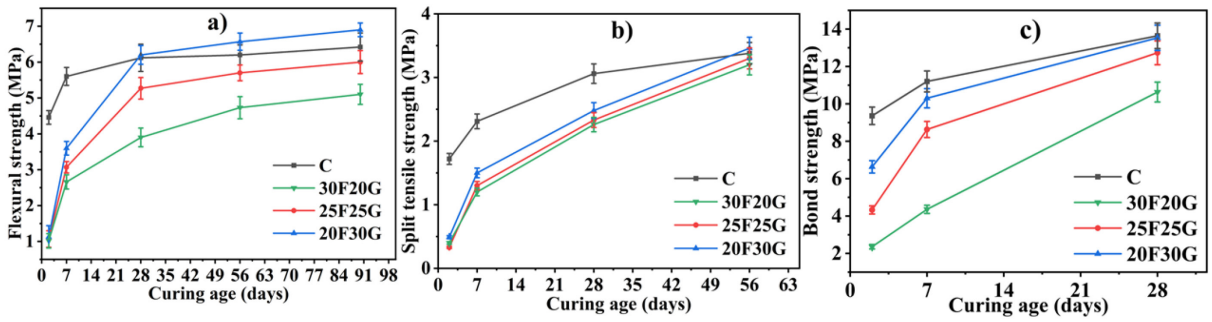

Fig. 3 a) Flexural strength, **b)** split tensile strength and **c)** bond strength development of control concrete and HVMAC mixes over curing time

3.5 Thermogravimetric analysis (TGA)

TG-DTG plots for each of the 28-day concrete samples are presented in Fig. 4a). The traces may be split into various stages, with three stages present in the control mix, and four stages visible in the traces for the HVMAC samples. The endothermic peak from 25 to 200 °C indicates the decomposition of multiple phases [50–53] including i) evaporation of free water (25-105 °C), ii) loss of bound water i.e., interlayer water in C-S-H (100-150 °C) [52], iii) dehydration of ettringite (AFt, 50-120 °C), and iv) decomposition of gypsum (Gy, 120-150 °C). Dehydroxylation of portlandite and decarbonation of calcium carbonate occurs at 400-500 °C and 600-800 °C, respectively. There is also gradual mass loss from dehydration of C-S-H

and C-A-S-H up to 600 °C without any significant feature in DTG curves [53,54]. The DTG curves for 25F25G, 20F30G, and 30F20G showed an additional endothermic peak from 225 to 325 °C, signifying the presence of hydrotalcite (Ht, $Mg_4Al_2(CO_3)(OH)_{12}.4H_2O$), arising from the presence of MgO in the slag [55].

From the obtained thermogravimetric mass loss (TG%) results, major hydrated phase compositions such as calcium hydroxide (CH), water-$_{related}$ to hydration products excluding CH (WH), calcium carbonate (CC) were quantified for all the 28-day samples using Equations 3, 4 and 5, respectively. Additionally, key deleterious compounds such as ettringite (AFt) and gypsum (Gy) formed due to the action of sulfate ions and Friedel's salt (Fs) due to chloride ions were quantified in the 28-day samples to set a baseline for non-exposed concrete samples using Equations 6, 7 and 8 [52,56,57].

$$CH\% = (\%W_{CH}) \times (\frac{M_{CH}}{M_{H_2O}}) = (\%W_{CH} \times \frac{74}{18}) \quad (3)$$

$$WH\% = W_T - W_{CH} \quad (4)$$

$$CC\% = (\%W_{CC}) \times (\frac{M_{CC}}{M_{CO_2}}) = (\%W_{CC} \times \frac{100}{44}) \quad (5)$$

$$\text{AFt (\%)} = W_{AFt} \times \frac{M_{AFt}}{26M_{H_2O}} \quad (6)$$

$$\text{Gy (\%)} = W_{Gy} \times \frac{M_{Gy}}{2M_{H_2O}} \quad (7)$$

$$\text{Fs (\%)} = W_{Fs} \times \frac{M_{Fs}}{6M_{H_2O}} \quad (8)$$

where, W_{CH}, W_{CC}, W_{AFt}, W_{Gy}, and W_{Fs} are the percentage mass loss corresponding to CH, CC, AFt, Gy and 6 moles of water from Fs at 400-500 °C, 600-800 °C, 50-120 °C, 120-150°C and 230-380 °C, respectively. M_{CH}, M_{H2O}, M_{CC}, M_{CO2}, M_{AFt} and M_{Gy} are the molecular weight of calcium hydroxide (74 g/mol), water (18 g/mol), calcium carbonate (100 g/mol), carbon dioxide (44 g/mol) and ettringite (786.7 g/mol), gypsum (172.17 g/mol) and Friedel's salt (561.3 g/mol), respectively. W_T is the total weight loss percentage for the 35–600 ˚C temperature range.

Fig. 4b) shows the quantified CH%, WH% and CC% for the 28-day control mix and all HVMAC samples. The portlandite and calcite contents were greater in the control concrete sample (C) than in the blended concrete samples. The increased calcite content in the control

mix is due to the presence of limestone in OPC, thus the lower levels in the HVMAC mixes can be attributed to dilution. Conversely, WH% was higher for HVMAC mixes than the control mixes due to the pozzolanic action of mineral admixtures to produce supplementary C-S-H by consuming the portlandite formed during hydration [58]. This also explains the depleted portlandite levels in the HVAMC samples. Fig. 4b) also shows that among all the HVAMC mixes '20F30G' mix showed a higher percentage of WH (i.e., 40% higher than that of control concrete) and lower concentration of CH and CC content (i.e., 15-20% higher to that of control concrete). This mix showed the best mechanical performance, showing the importance of the pozzolanic reaction in defining performance.

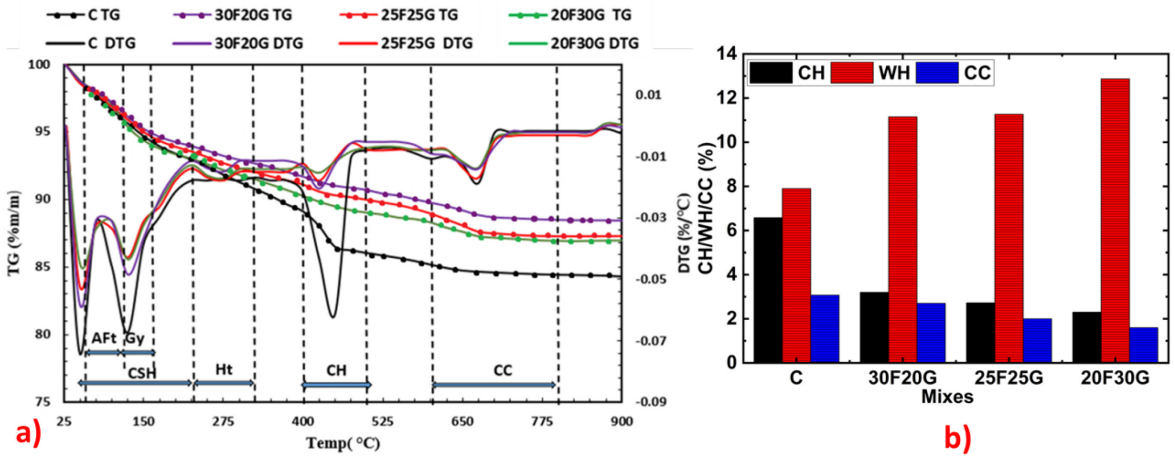

Fig. 4 a) TG-DTG plot of 28 days cured concretes**, b)** Phase compositions quantification of 28 days cured concretes

3.6 Fourier transform infrared spectroscopy (FTIR)

FTIR spectra for all samples cured for 28 days are presented in Fig. 5a).

The asymmetric deformation and wagging vibration of CO_3^{2-} in calcite is indicated by the bands cantered at 1412-1453 cm^{-1} and 874 cm^{-1}, respectively [59,60]. The control mix has a stronger calcite peak than mixed mixes, which can be attributed to the higher clinker percentage. The vibrations of Si–O in the C–S–H and S–O groups are represented by vibration bands 973 cm^{-1} and 1084 cm^{-1}, respectively [61]. The band associated with C-S-H was found to be intense for the mix comprising of higher GGBFS composition. The Si–O–Si cross-linking bonds are present in the band at about 774-776 cm^{-1}, which corresponds to the C-S-H phase composition [61]. The same was strengthened with the increase in GGBFS concentration in the mix.

3.7 Durability performance of HVMAC

3.7.1 Sorptivity test

Concrete is a porous medium with a capillary pore system, which allows moisture and deleterious ions to ingress into the concrete [62]. Capillary sorption was calculated as initial sorption rate (1º) and secondary sorption rate (2º) as per ASTM C1585. The initial sorption rate (1º) was calculated over the first 6 hours using the slope of the sorption (I) curve versus the square root of time (mm/s$^{0.5}$). The secondary sorption rate (2º) was determined for immersion beyond 1 day. These data for the control and all HVMAC mixes, after curing for 14 and 28 days, are shown in Fig. 5b).

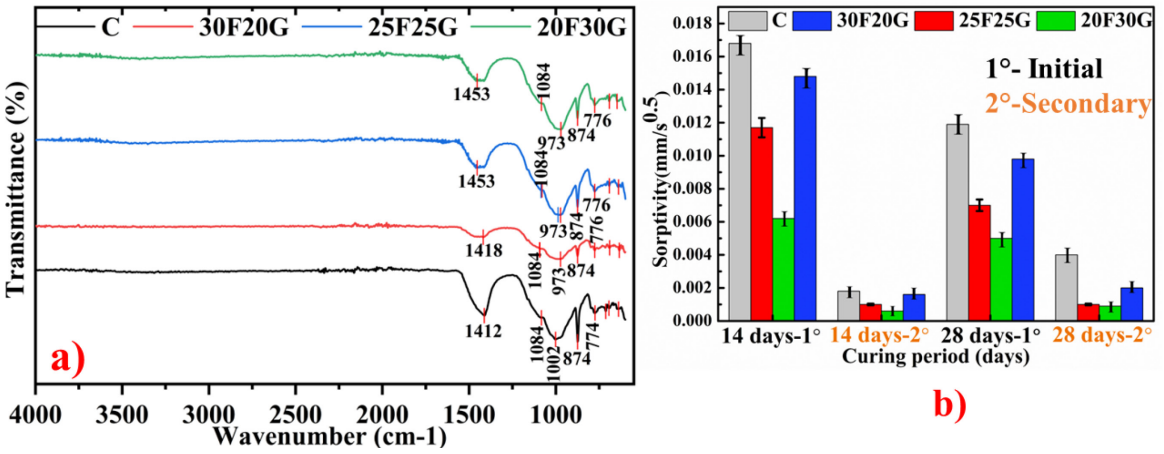

Fig. 5 a) FTIR spectrum for 28 days water-cured concretes**; b)** initial sorption rate (1º) and secondary sorption rate (2º) of 14 days and 28 days cured concretes

The control concrete showed highest sorptivity after both curing durations, significantly higher than for any of the HVMAC mixes. This is due to the pozzolanic and hydraulic behaviour of the mineral additions, leading to a more refined pore structure by reducing the interconnected capillary pores and therefore reducing the susceptibility to capillary suction [62]. This is supported by the reduced portlandite contents and increased bound water contents measured by TGA. Furthermore, sorptivity fell with increasing GGBFS content, reflecting the greater reactivity of GGBFS than FA.

The secondary sorptivity values for all mixes were significantly lower than the initial sorptivity values, with the trends between different mixes being similar to the primary values. Initial water sorption into concrete is spontaneous, with air being displaced by water within 6 hours. However, not all air is displaced during the initial stage and so this leads to secondary sorption, where the trapped air gets dissolved in water, and diffuses into unsealed peripheral surfaces where upon it escapes slowly (from 1 to 7 days). Eventually, the sample reaches saturation when all entrapped air within the material is lost [63].

3.7.2 Aggressive exposure

To check the durability of HVMAC mixes against aggressive ions, specimens were variously exposed to acids, chlorides and sulphate solutions. The results are reported in the following sections,

3.7.2.1 Acid test (5% H_2SO_4)

The changes in compressive strength and mass upon immersion in sulphuric acid are shown in Figs 6 and 7, respectively. All samples lost compressive strength with progressive acid exposure (Fig. 6). However, the strength loss was less for the HVMAC samples than for the control mix, and again, the performance correlated with the GGBFS content, with mix 20F30G performing best of all. The improved performance can be attributed to the pozzolanic reaction leading to a denser, more refined microstructure [64].

The compressive strength of HVMAC mixes was found to be lower than that control mix irrespective of the exposure period of 14 days cured samples. However, contrasting results were found for specimens cured for 28 days. Here, the compressive strength of the control concrete was seen to be lower than that of the HVMAC mix. Among the HVMAC mixes, mix '20F30G' with the highest GGBFS content showed better resistivity to acid solution. It is reported that water-to-binder ratio, curing, mineral admixture dosage etc., are all important factors that influence resistance to acid attack. The lower resistivity of HVMAC mixes to acid solution was attributed to inadequate curing. This is because of the slow initial reactivity of fly ash and GGBFS and at the initial stage of cement hydration, these mineral admixtures contribute mostly as a filler rather than taking part in reactivity. It can be understood from the results that the optimistic performance of HVMAC mixes cured for 28 days was due to the involvement of fly ash and GGBFS in pozzolanic and hydraulic reactivity [64]. Further, at the curing of 28 days, HVMAC mix would have attained a dense microstructure due to the consumption of porous calcium hydroxide to dense C-S-H.

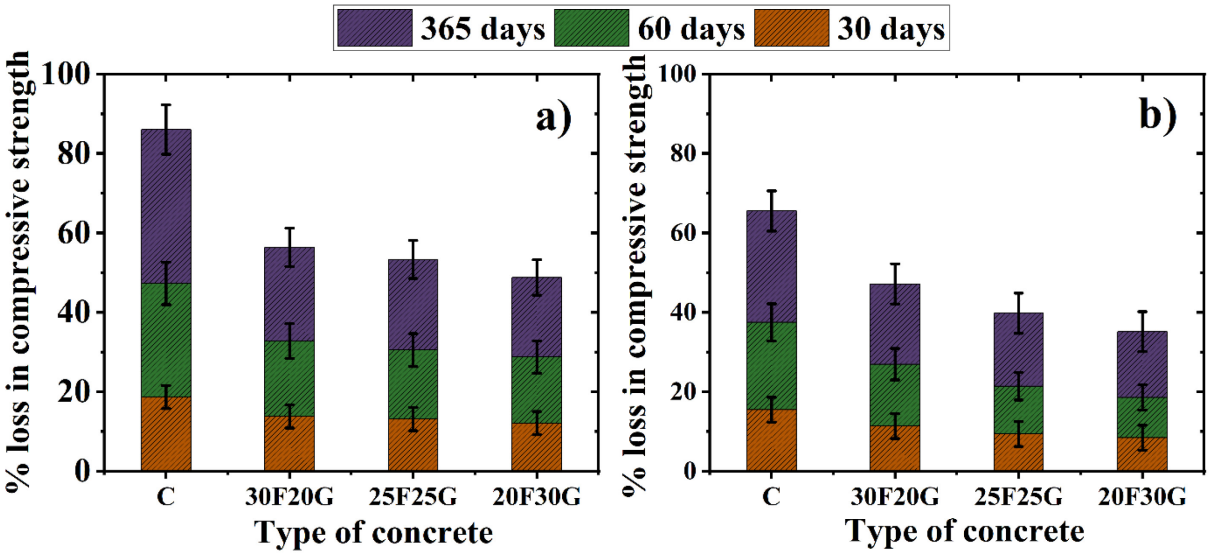

Fig. 6 Percentage loss in compressive strength of the various mixes upon exposure to H_2SO_4 solution, in samples cured for a) 14 days and b) 28 days

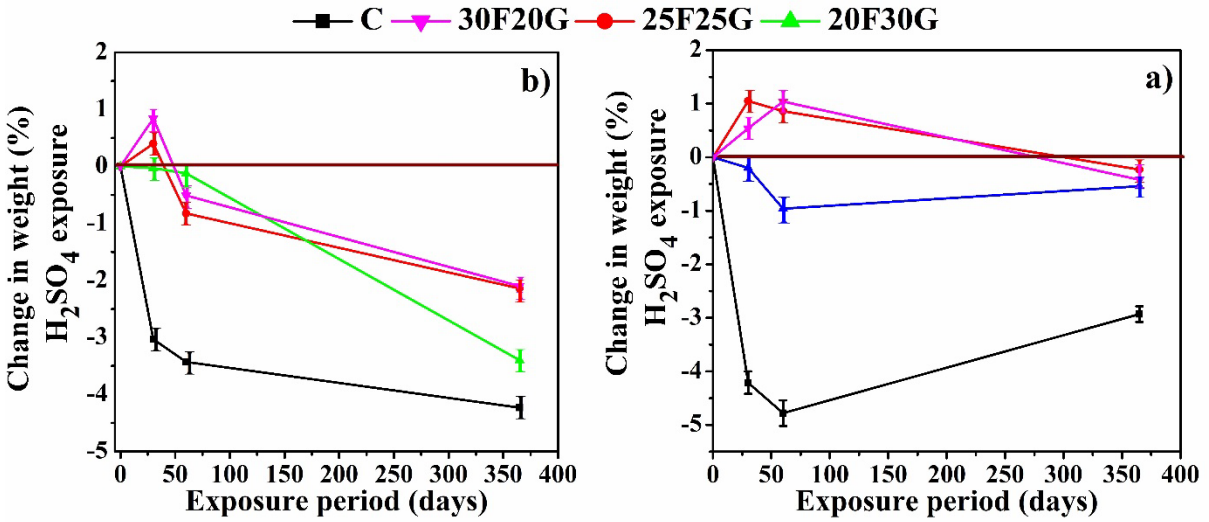

Fig. 7 Percentage mass change of various types of concretes exposed to H_2SO_4 solution, in the samples cured for a) 14 days and b) 28 days

Acid immersion leads to the degradation of concrete, but there can be contradictory phenomena. Reactions between the alkaline cement paste and the acid can lead to dissolution (and so mass loss) or precipitation of insoluble reaction products (and so a mass gain).

All of the samples cured for 14 days showed an eventual mass loss, with the control mix performing worst. Within 28 days the control mix had lost about 3% mass. The HVMAC mixes meanwhile showed minimal loss to 56 days, with the FA-rich mixes even showing an initial increase in mass. This increase in weight may be attributed to reactions between the sulphuric acid and the hardened cement paste, for example with portlandite to produce gypsum and with

aluminates in the cement to form ettringite [58]. The higher aluminate content of the GGBFS and particularly the FA suggest the formation of ettringite. Given the low sorptivity of the HVMAC mixes, these reactions were likely just at the surface of the concrete, also minimising the loss of material due to spalling.

It can be observed from Fig. 7 that in the case of concrete cured for 14 days and exposed to sulphuric acid, control concrete (C mix) showed weight gain with progressive exposure. The trend of increase in weight was found to be rapid for the first 30 days of exposure and then the rate of increase in weight was seen to be reduced gradually. In the case of HVMAC concrete mixes increase in weight was found to intensify at 365 days of acidic exposure. This increase in weight was attributed to the associated chemical reaction of sulphuric acid with cement hydrates such as calcium hydroxide to form gypsum and further converted to ettringite leading to the increase in volume [47]. Further, this phenomenon also depends on the concentration and pH of the sulphuric acid solution. Higher the acidity, larger would be the acid cement reaction as well as the weight gain associated to the formation of gypsum and ettringite. Therefore, weight loss study may not be an appropriate measurement to indicate the level of deterioration in concrete specimens exposed to sulphuric acid. However, compressive strength loss and relevant characterization techniques would provide more consistent information to understand the resistance of a mix against acid attack [65].

To understand the changes in phase assemblage better, characterization by TGA and FTIR was undertaken. Fig. 8a) presents the TG-DTG curves of concrete samples cured for 28 days and subjected to 365 days of sulphuric acid attack.

Acid immersion led to significant changes in the phase assemblages, evidenced by the TG-DTG plots (Fig. 8a)) compared to those from the non-exposed samples (Fig. 4a)). In particular, changes were considerable over the temperature range 25 to 300 °C. The endothermic peak at 120-150 °C corresponding to the decomposition of gypsum (Gy) was much more intense. This is due to the reaction of sulphuric acid with C-S-H and CH in the hardened cement paste to form voluminous, soft, secondary gypsum (Gy). At pH < 4.5, sulfuric acid directly attacks the major hydration product i.e., C-S-H to form soft soluble gypsum and silica gel [66]. Formation of secondary ettringite can be noticed in the range of 50-120 °C. There was also a dramatic decrease in the intensity of the endothermic peak corresponding to hydrotalcite (Ht) after acid exposure.

The amount of hydration products such as calcium hydroxide (CH) and water-related hydration products excluding CH (WH) and calcium carbonate (CC) were quantified for sulphuric acid exposed samples using Equations 3-5 and presented in Fig. 8b).

The amount of hydration products quantified for the concrete samples that were exposed to 365 days of acid solution showed a tremendous decrease in CH and WH content in control mix (C). This is caused due to the interaction of major hydration compounds such as CH and C-S-H with sulphuric acid to form a soft soluble secondary gypsum compound. However, WH % was found to be higher than that of CH% irrespective of mix type. This is due to the fact that quantification of WH% corresponds to the temperature range of 35-600 ºC also relates to the dehydration of other hydration products such as C-A-S-H, C-A-H and alumina silicate phases containing magnesium [57]. It is to be noted that there is not much drop in CH% and WH% for 20F30G mix exposed to 365 days of acid solution with respect to that of non-exposed mix (refer Fig. 4b)). This indicated the higher resistivity of the mix against the sulphuric acid attack owing the increased reactivity and possible filler effect in the concrete system. Further, there is not much variation in the calcium carbonate (CC) content noticed with respect to non-exposed samples.

Considering, gypsum and ettringite as the major deleterious compounds responsible for the deterioration of concrete exposed to sulphuric acid, these compounds were quantified (using Equations 6-7) and presented in Fig. 8c).

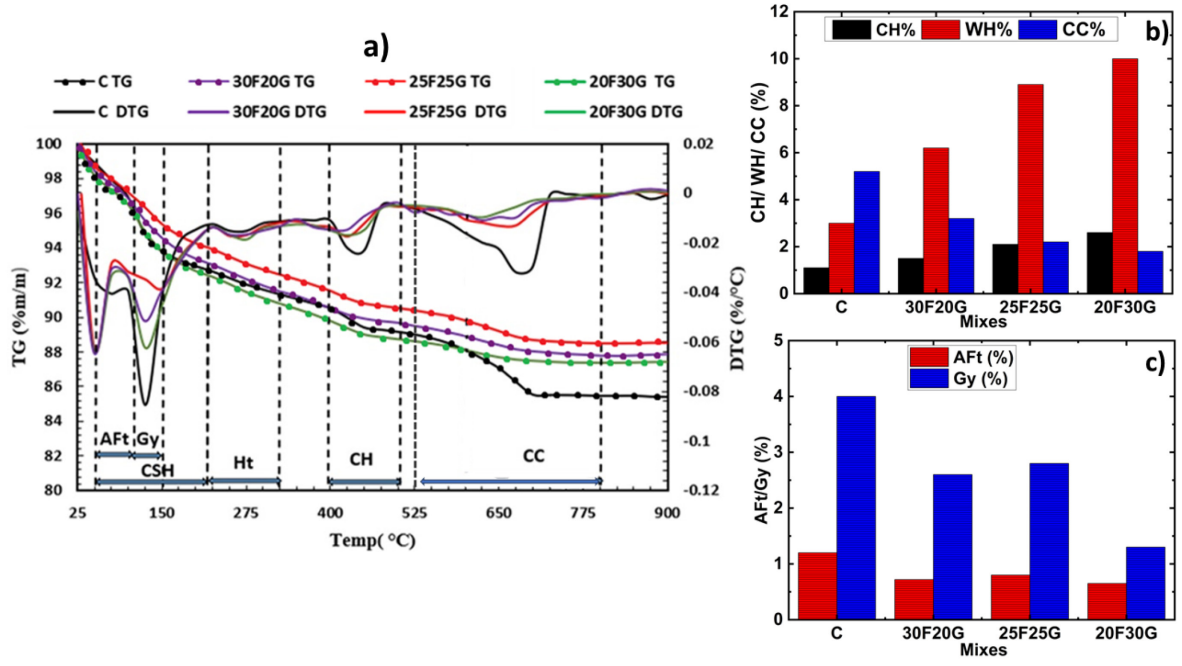

Fig. 8 a) TG-DTG plot acid exposed concretes, **b)** Quantified amount of CH, WH and CC, **c)** Quantified amounts of ettringite (AFt) and gypsum (Gy) of 365 days acid exposed concretes

The gypsum and ettringite contents were higher in the control mix than in the HVMAC mixes. It is to be noted that the amount of secondary Gy formed is higher compared to that of secondary AFt indicating the interaction of gypsum with aluminate phase (C_3A) has not taken place significantly. Secondary gypsum is soft and highly soluble which leads to the loss of binding property. Hence, its extent of formation influences the level of deterioration in terms of strength/weight.

The lowest quantity of AFt and Gy was seen for the mix '20F30G' with 30% GGBFS i.e., 55 and 50 % lower than that of control mix (C), respectively. This is ascribed to the improved reactivity and filler effect in the concrete system owing to the synergetic action of multiple mineral admixtures.

FTIR spectrums obtained for all the mixes exposed to 365 days of sulphuric acid solution are presented in Fig. 9.

FTIR spectra of concrete mixes exposed to sulphuric acid show major vibration bands at the wavenumbers of 1445-1464 cm^{-1}, 1084-1113 cm^{-1}, 972-1004 cm^{-1}, 874 cm^{-1}, 776 cm^{-1} and 663-669 cm^{-1} conforming to C-O bonds of carbonate phases, asymmetric stretching vibration of function group of sulfates (SO_4^{2-}), Si-O stretching bond of C-S-H phase, and C-O bonds of carbonate phases, symmetric stretching vibration of Si-O-Si, and presence of SO_4^{2-} bonds respectively [61,67].

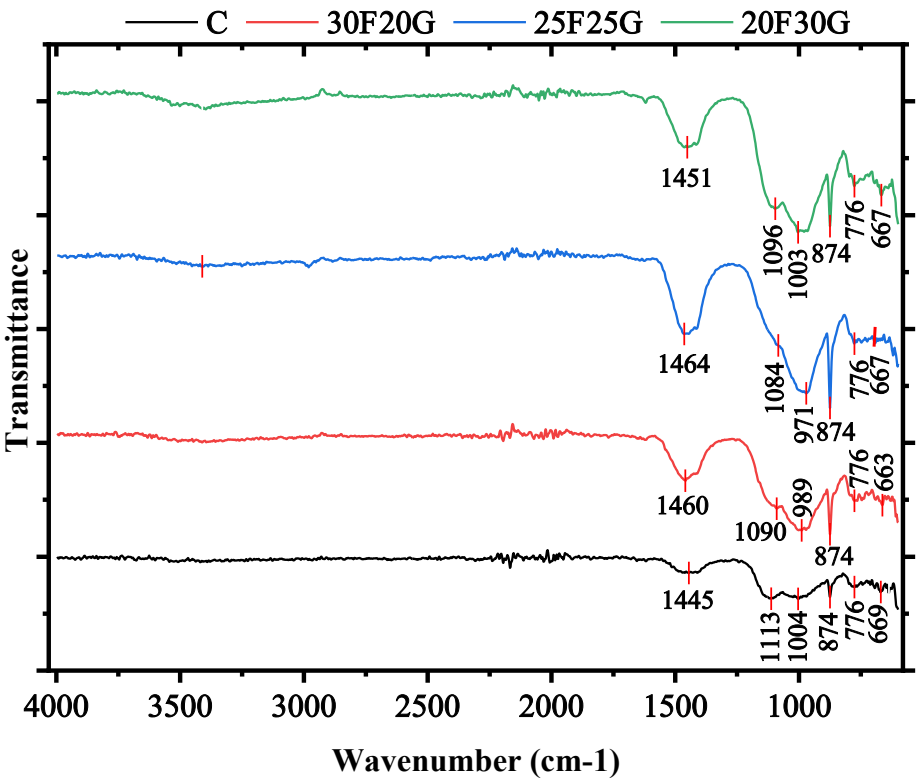

Fig. 9 FTIR spectrum of concrete samples exposed to sulphuric acid for 365 days

The peak corresponding to C-S-H vibration at 972-1004 cm^{-1} was found to be broad for C, and 25F25G mixes. The connecting peak to C-S-H vibration (969 cm^{-1}) at 1084-1113 cm^{-1} confirms the occurrence of SO_4^{2-} (deleterious compound formed due to sulphuric acid attack) that was found to be prominent in control, 25F25G and 30F20G mixes. While 20F30G mix showed negligible peak intensity at 1096 cm^{-1} indicating the least formation of gypsum and this result is in line with the obtained TGA results. The presence of SO_4^{2-} weak bond at 662 cm^{-1} confirms the occurrence of sulfate species [68].

3.7.2.2 Sulphate attack test (5% $MgSO_4$)

Figs 10 and 11 demonstrate the percentage change in compressive strength and percentage change in weight of concrete mixes cured for 14 and 28 days when exposed to 5% $MgSO_4$ solution for 30, 60 and 365 days.

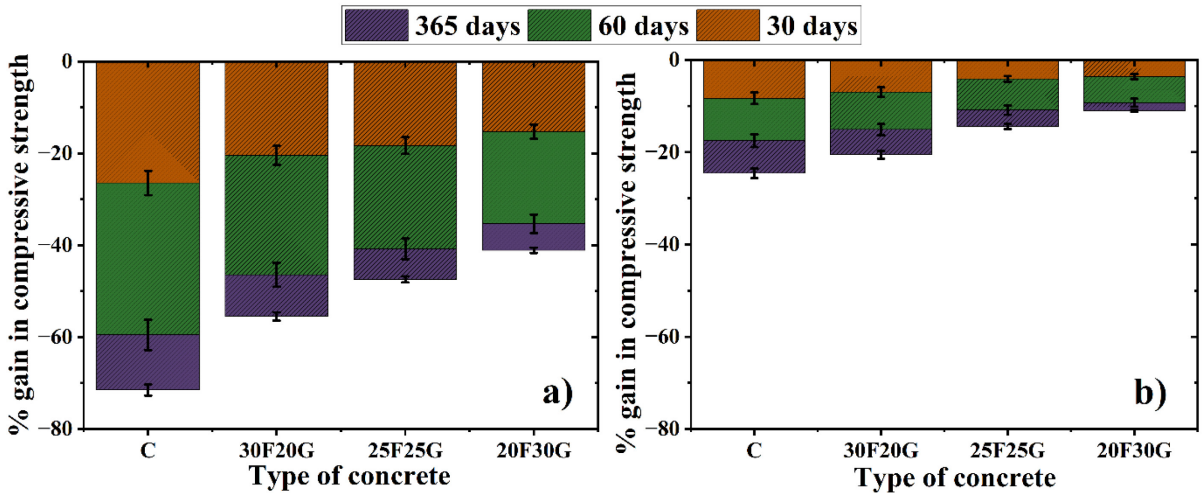

Fig. 10 Percentage loss or gain in compressive strength of HVMAC mixes exposed to $MgSO_4$ solution cured at a) 14 days and b) 28 days

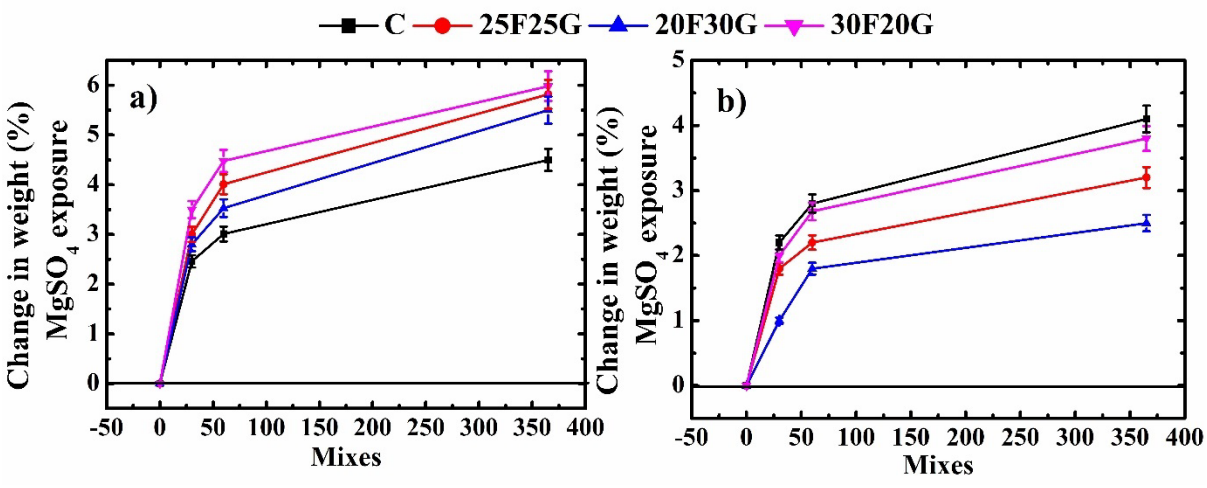

Fig. 11 Change in weight percentage of HVMAC mixes exposed to $MgSO_4$ solution in a) 14 days cured and b) 28 days cured samples

There was an initial increase in compressive strength upon immersion in $MgSO_4$ solution, followed typically by a drop in strength by 365 days. This is due to expansive gypsum and ettringite formation from portlandite and AFm phases in the cement. These reactions fill the pore spaces and increase compressive strength [69]. A further reason could be the blocking effect from the formation of brucite (Mg^{2+} + CH = $Mg(OH)_2$) in cement matrix [70]. The subsequent strength reduction by 365 days is due to cracking from expansive stresses caused by the voluminous ettringite. It was also reported that exposing the Portland cement system to magnesium sulphate solution surface double layer comprising of layer of brucite and gypsum layers one after the other possibly forms [71]. It is also stated that the formed double layer for

493 the magnesium sulphate solution exposed concrete specimens undergoes excessive expansion
494 pressure in the cement matrix [70].
495 The HVMAC samples performed better than the control mix. This is due to a number of factors.
496 Their lower permeability prevents the ingress of deleterious species. They also have lower
497 portlandite contents, inhibiting gypsum formation. Finally, despite the increased aluminate
498 contents of both GGBFS and FA, this aluminium is incorporated into the C-S-H and as
499 hydrotalcite so is not necessarily available for production of ettringite. This was supported by
500 TGA/DTG analysis of the specimens.

501 Samples cured for 28 days, particularly HVMAC specimens, showed better resistance to the
502 $MgSO_4$ solution. This is due to the more gradual reactivity of the mineral admixtures compared
503 to cement clinker, and pore structure refinement. Among the HVMAC mixes '20F30G' mix
504 showed the best resistivity to sulphate attack. This can be attributed to the presence of greater
505 proportion of GGBFS, which offers excellent resistance sulphates.

506 The highest mass loss associated to sulphate attack caused by $MgSO_4$ solution was seen for
507 HVMAC mixes cured for 14 days compared to control concrete (Fig. 11). However, results
508 were found to be converse when 28 days cured concrete specimens were exposed to $MgSO_4$
509 solution. The mass loss is greatest for the HVMAC mixes at 14 days because the slow rate of
510 hydration results in an open pore structure. Meanwhile, after curing for 28 days, the specimens
511 were impermeable and so resisted $MgSO_4$ ingress. It is also important to note that '20F30G'
512 mix showed the least mass loss at all the exposure periods because GGBFSFS is more reactive
513 than FA and known to aid sulphate resistance.

514 TGA and FTIR analysis were subsequently carried out to examine phase changes upon
515 exposure to $MgSO_4$ for 365 days and the results are shown in Fig. 12a) and Fig. 13,
516 respectively.
517 As with exposure to sulphuric acid, exposure to $MgSO_4$ led to increased presence of gypsum
518 in all samples. In addition, the small endothermic peak observed at the temperature range of
519 325 to 400 ºC is attributed to the dehydroxylation of brucite ($Mg(OH)_2$). However, magnesium
520 ions can also interact with C-S-H to form M-S-H (magnesium silicate hydrate) which disturbs
521 the cohesive properties of the concrete [71]. Thus, only traces of brucite are observed in the
522 samples. Furthermore, in the case of the HVMAC samples, there was also overlap with the
523 peak due to hydrotalcite.

The DTG peak related to the decomposition of secondary ettringite can be noticed in the temperature range of 50-120 °C. It is also important to note that as the characteristic decomposition boundary of ettringite and C-S-H overlaps, the quantity of ettringite formed alone cannot be considered as the deterioration indicator. However, the characteristic decomposition peak of gypsum was seen to be very prominent and that was considered as a chief indicator of the deterioration extent.

Quantification was carried out on the major hydration products CH, water corresponding to hydration products excluding CH (i.e., C-S-H, AFM, CAH, CASH, etc.,) and calcite for the specimens exposed to magnesium sulphate using Eqs 3-5 (Fig. 12b)). Further, soft, less dense, soluble-white gypsum phase component and secondary ettringite traces were also quantified as per the Eqs. 6-8 (Fig. 12b)).

The quantified amount of calcium hydroxide for magnesium sulphate-exposed concrete samples (Fig. 12b)) was found to be reduced compared to that of non-exposed samples (refer Fig. 4b)). This is mainly attributed to the reaction of CH with sulphate ions to form compounds such as secondary gypsum and brucite. The reduction in CH content in control mix was principally associated to the aforementioned reaction mechanism. However, lower percentage of CH in all HVMAC samples was ascribed to the pozzolanic reactivity of siliceous and aluminous mineral admixture with calcium hydroxide component. Water related to hydration products was also found to be reduced significantly in control sample. Magnesium sulphate reaction in the pore solution of concrete even attacks C-S-H more rapidly than sodium sulphate solution due to the formation of M-S-H (lower binding ability). However, the influence of magnesium sulphate on the WH percentage of HVMAC mixes was seen to be less significant. This clearly indicates the resistance of the mixes against the sulphate attack. Calcite percentages were seen to be lower and not much difference was observed when compared to that of non-exposed mixes. Among all the mixes ‘20F30G’ mix showed lesser disturbance in concrete hydration system. CH%, WH% and CC% values for ‘20F30G’ mix at 365 days of $MgSO_4$ solution exposure were seen to be 2.2%, 10.2% and 2%, respectively showing lesser variation in correspondence to non-exposed ‘20F30G’ mix amongst all mixes.

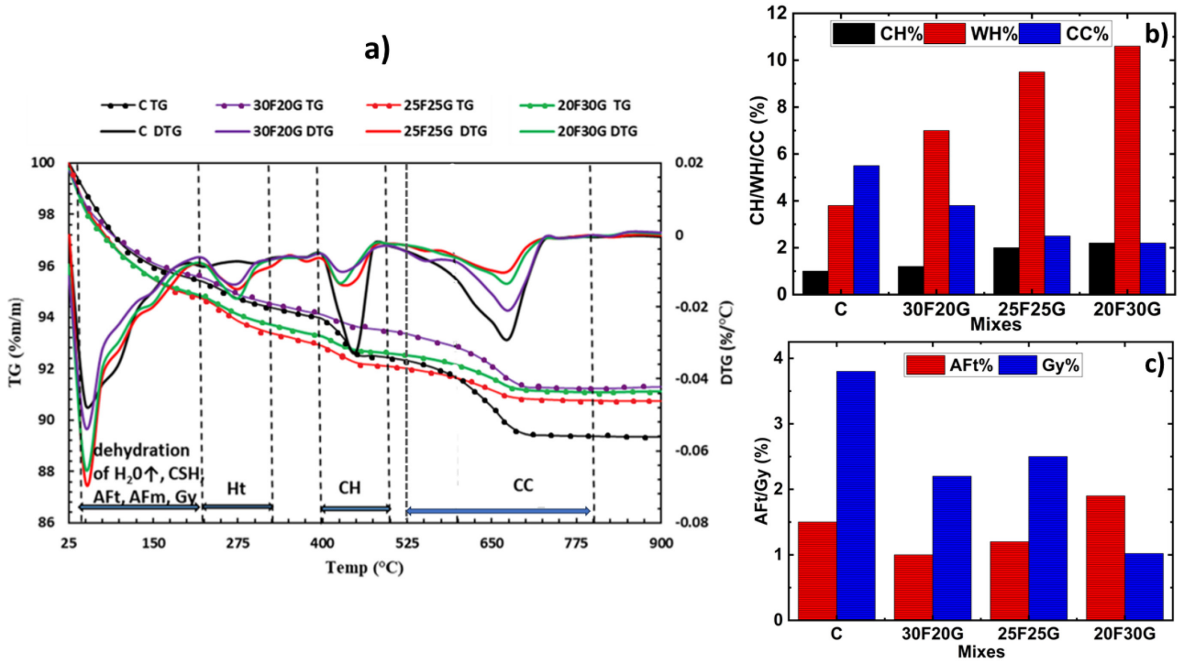

552

553 **Fig. 12 a)** TG-DTG plot for concretes exposed to sulphate medium, **b)** Quantified amount of

554 CH, WH and CC, **c)** Quantified amounts of ettringite (AFt) and gypsum (Gy) in 365 days

555 sulphate exposed concrete

556 It can be inferred from Fig. 12c) that the quantity of ettringite formed due to $MgSO_4$ exposure
557 was found to be lower than H_2SO_4 exposure. This indicates that substantial reaction gypsum
558 (formed due to the reaction of sulphate ions and portlandite) with tri-calcium aluminates phase
559 was not sulphate to form expansive ettringite. Therefore, the $MgSO_4$ reaction with phases
560 (such as CH and C-S-H) in concrete pore solution is characterized by the formation of gypsum
561 in a similar manner to that of sulphuric acid attack, and it leads to the swelling action in concrete
562 [47]. On the other hand, secondary ettringite (AFt) formation in the concrete exposed to $MgSO_4$
563 solution was found to be negligible. This was due to the occurrence of reaction between CH
564 and C-S-H phases with $MgSO_4$ to form gypsum along with magnesium hydroxide (brucite)
565 resulting in lower resolution as well as pH value of the magnesium hydroxide. The occurrence
566 of this mechanism weakens the stability of the ettringite and calcium–silicate–hydrate (C–S–
567 H). It is for that reason ettringite formation was found to be lower than that of gypsum
568 concentration in the $MgSO_4$-exposed concrete samples.

569 Among all mixes, control concrete showed higher formation of Gy specifying the least
570 resistance towards sulphate attack. This can be ascribed to the relatively higher percentage of
571 CH content in the case of Portland concrete compared to that of HVMAC samples. Mineral

admixture-based concrete samples comprise of lesser concentration of lime compared to that of the control sample and thus reduce the reactive C_3A and $Ca(OH)_2$ content in the pore solution of the concrete system. It is reported that considerably higher concentrations of C_3A content in cement are more prone to sulphate attack [72]. Integration of silica-rich minerals minimizes the load of portlandite in concrete leading to the formation of secondary stable C–S–H. It is for that reason all HVMAC mixes showed lower percentage of Aft and Gy content in the concrete and therefore found to have better resistance against sulphate attack. Similar to sulphuric acid attack, in the case of magnesium sulphate attack also '20F30G' mix reflected the least percentage of AFt and Gy formation thereby specifying the imperviousness towards aggressive sulphate ions.

Fig. 13 demonstrates the FTIR spectra of concrete samples exposed to magnesium sulphate for 365 days.

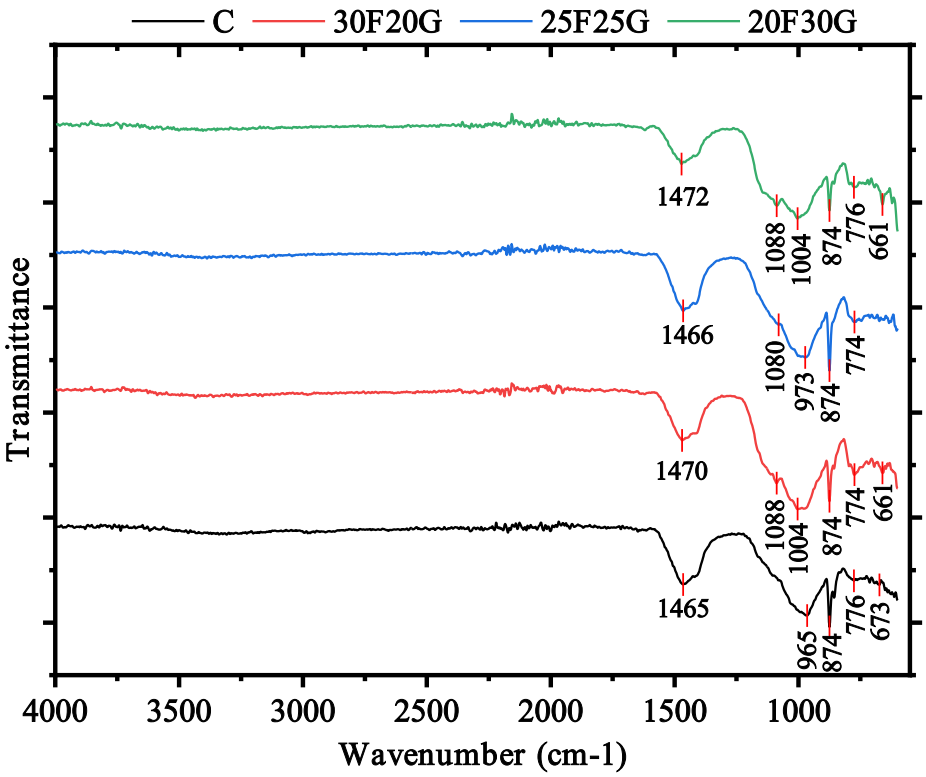

Fig. 13 FTIR spectrum of concrete samples exposed to $MgSO_4$ for 365 days

It can be characterised from the obtained FTIR spectra for $MgSO_4$ exposed concrete that there exist multiple characteristic bands at various wavenumbers corresponding to the different chemical bonds similar to the samples exposed to H_2SO_4. It can be observed from Fig.13 that there is a strong characteristic band at the wavenumber of 965-1004 cm^{-1} that relates to the Si–

O stretching vibrations. The shoulder peaks at 1080-1088 cm^{-1} and 774-776 cm^{-1} correspond to SO_4^{2-} stretching vibrations, which can be attributed to the ingression of magnesium silicate leading to the formation of gypsum/ ettringite phases. It is reported that the characteristic vibration band of Mg–O stretching vibration exists at 459 cm^{-1} [73]. But, in this study, as the wavenumber range of FTIR equipment was fixed from 500 to 4000 cm^{-1}, this result was unable to be depicted in Fig. 13. Further a strong vibration band at 1455 cm^{-1} links to the C=O bending vibration of the carbonates. The characteristic band at 750 cm^{-1} was attributed to the C-O bonds of carbonates.

5.2.3 Chloride test (NaCl immersion test)

Exposure to NaCl solution for 30, 60 and 365 days led to the loss in strength and loss of mass, which are represented in Figs 14 and 15, respectively.

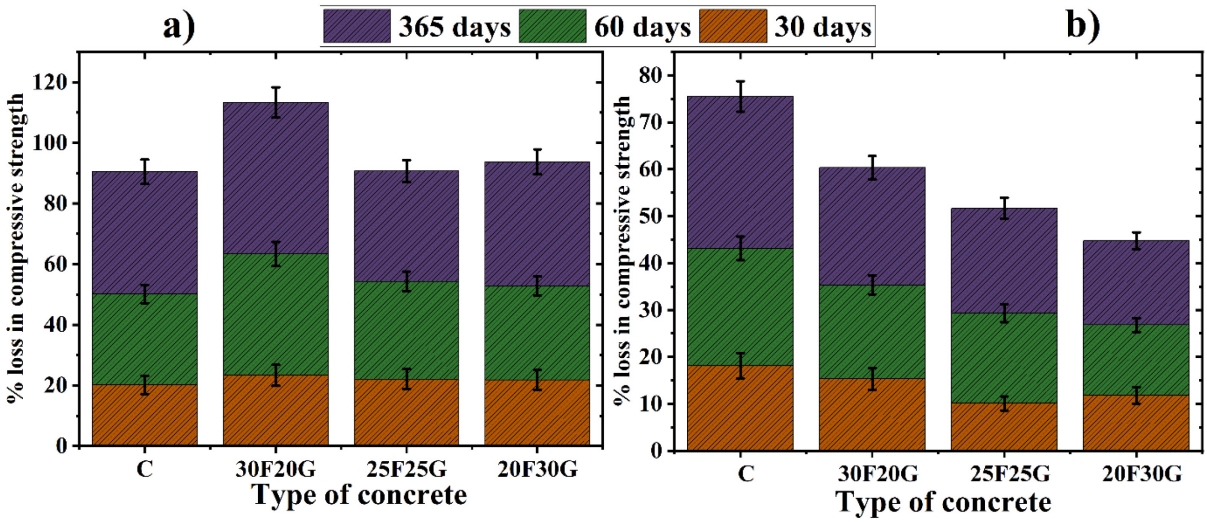

Fig. 14 Compressive strength variation of HVMAC mixes exposed to NaCl solution in a) 14 days cured and b) 28 days cured concrete samples

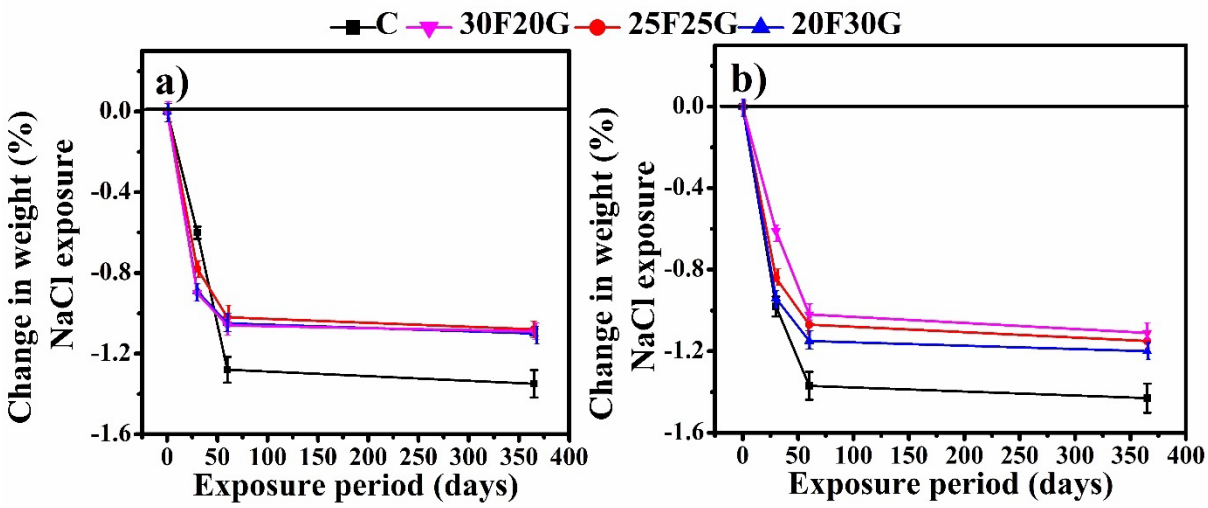

Fig. 15 Change in weight percentage of HVMAC mixes exposed to NaCl solution in a) 14 days cured and b) 28 days cured concrete samples

The drop in the compressive strength of concrete specimens after exposure to NaCl solution for designated period was generally consistent for both the curing ages specimens (Fig. 14). It can be perceived from the figure that 14 days cured control concrete showed higher resistance to NaCl solution. This is caused due to the incomplete reactivity in HVMAC mixes as a result of dilution effect. However, results were found to be in contrast for 28 days cured concrete specimens and highest resistance to NaCl solution was offered by HVMAC mixes. This is due to the improved microstructure HVMAC mixes due to the occurrence of supplementary reaction in addition to the filler action of mineral admixture at the curing age of 28 days. The change in compressive strength mainly relies on certain aspects such as cement hydration, supplementary reaction in terms of alternative binder system, curing age, Cl^- concentration in the salt solution, and duration of attack. Diffused Cl^- ions react with the hydration phases in concrete thereby influencing the pore volume, morphology and ITZ characteristics of concrete leading to the difference in development of cracks in concrete. Long-term exposure of concrete to NaCl solution showed certain variations in the failure. Similar to H_2SO_4 and $MgSO_4$ results, the lowest deterioration in terms of strength was observed for '20F30G' cured for 28 days.

It can be observed from Fig. 15 that the change in weight for both 14 and 28-day cured concrete specimens was found to be at similar rate up to the initial chloride exposure period of 30 days and 60 days. However, a large variation in the rate of change in weight corresponding to various mixes was observed at the exposure age of 365 days. In case of 14 days cured concrete specimens, control mix exhibited a lower change in weight among all concrete specimens and

627 the highest change in weight was observed for '30F20G' mix. This is because of the fact that
628 the weight of concrete relies on the hydration products, deleterious compounds formed due to
629 the ingression of Cl^- ion and the loss in binding property of concrete powders. As the curing
630 period of 14 days is not sufficient enough to promote the supplementary reaction of mineral
631 admixture, HVMAC mixes attain less dense matrix compared to that of non-diluted control
632 concrete. It is for that reason, diffusion of Cl^- ion intensifies for HVMAC mixes leading to the
633 larger mass loss. However, HVMAC mixes comprising of larger fraction of GGBFS content
634 (20F30G mix) showed only 8% higher weight loss compared to control. This was attributed to
635 the hydraulic property of GGBFS particles, which could initiate the reactivity quite earlier
636 compared to that of fly ash-rich HVMAC mix. It is to be noted that the results of weight change
637 were found to be in contract for 28 days cured specimens. This clearly indicates the refined
638 microstructure of concrete owing to the influence of mineral admixture on the reactivity of
639 concrete.
640 To determine the change in the phase composition of concrete attacked by NaCl solution
641 TG/DTG analysis was carried out. Fig. 16a) shows the TG/DTG plot of concrete samples
642 exposed to sodium chloride solution for a period of 365 days.
643 The TG-DTG plots revealed a broad endothermic peak over the temperature range 230-380 ºC
644 associated with Friedel's formed from the reaction of chloride ions with calcium aluminate
645 phases [43,55]. For the HVMAC mixes, this peak overlapped with that due to hydrotalcite.
646 Despite this, it was clear that the peak due to Friedel's salt was much weaker in the HVMAC
647 mixes than in the control mix (C).

648 Quantified amount of hydration compounds such as CH, CC and water corresponding to other
649 hydration products (i.e., C-S-H, AFm, CAH, CASH, etc.,) for the specimens exposed to 365
650 days of sodium chloride solution is presented in Fig. 16b). Further, Friedel's salt formed due
651 to the action of chloride ions with that of hydration products was calculated using Equations 8
652 and presented in Fig. 16c).
653 From Fig. 16b) it can be seen that similar to sulphuric acid and magnesium sulphate attack,
654 chloride ion (Cl^-) from sodium chloride solution also attacks calcium hydroxide phase in the
655 pore solution. During this mechanism, calcium cation from the $Ca(OH)_2$ was taken off to form
656 calcium chloride compound and formed calcium chloride reacts with calcium aluminate (C_3A)
657 in cement leading to the formation of voluminous reaction products called Friedel's salt
658 ($C_3A.CaCl_2.10H_2O$). It is for that reason, the quantified amount of CH content was found to be
659 reduced in the case of chloride-attacked concrete sample (Fig. 4b)). Quantified amount of

bound water except CH i.e., WH% and calcium carbonate (CC) percentage was also found to be reduced. It is well understood by the researchers that the formation of Friedel's salt replaces CO_3^{2-} or SO_4^{2-} from monocarbonate ($C_3A{\cdot}CaCO_3{\cdot}11H_2O$) and monosulfate ($C_3A{\cdot}CaSO_4{\cdot}12H_2O$) by Cl^- ions [71,72]. However, the effect of chloride on the amount of WH content for HVMAC mixes was noticed to be less significant than the control mix. This is attributed to the formation of stable secondary C-S-H by consuming portlandite from the concrete system.

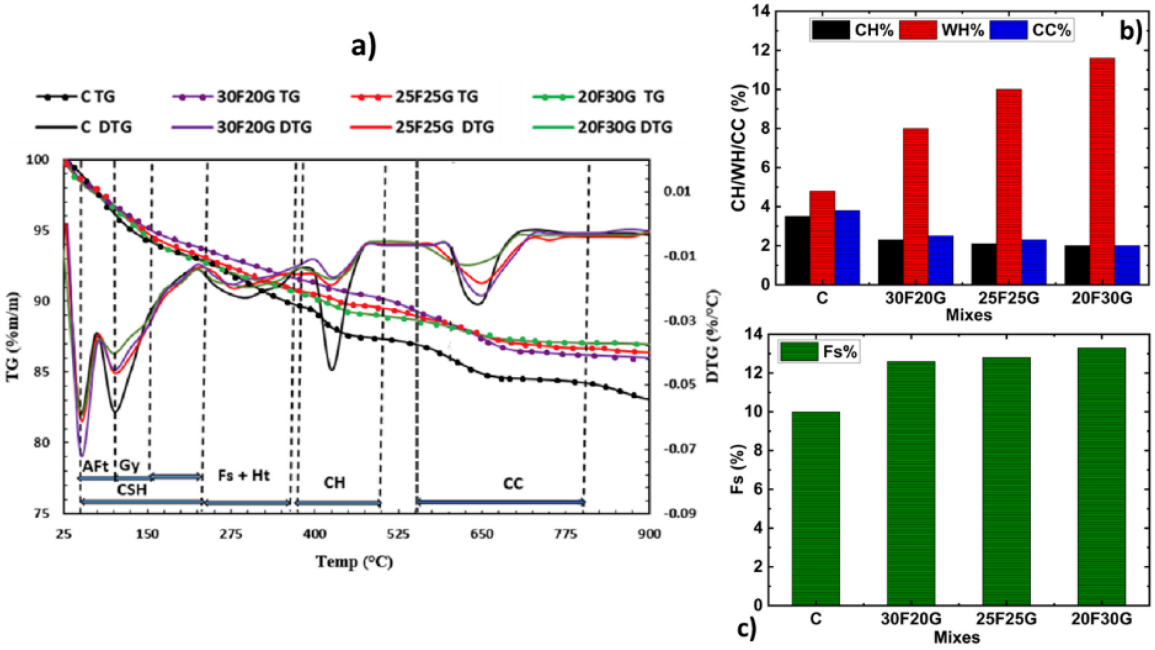

Fig. 16 a) TG-DTG plot for concretes exposed to chloride medium, **b)** Quantified amount of CH, WH and CC, **c)** Quantified amount of Friedel's salt (Fs) in 365 days chloride exposed concretes

The amount of formation Friedel's salt was found to be increased for all HVMAC mixes. This is due to the higher concentration of Al_2O_3 composition in mineral admixture. As chloride binding in the NaCl-attacked concrete system is dependent on the phase composition of concrete it corresponds to the aluminate phases in concrete such as C_3A, C_4AF, monocarbonate, C-A-H and C-A-S-H. From this result, it is confirmed that Al_2O_3 contributes to the chloride binding mechanisms to form Friedel's salt [74]. However, studies report that the chemical binding of chloride ions gradually diminishes due to the carbonation activity [74]. Hence, it is always important to understand the carbonation mechanism along with chloride attack to understand the effect on concrete for long-term practical applications.

For further verification of the chloride-attacked concrete samples, FTIR analysis was carried out and the obtained results of 365 days exposed samples are presented in Fig. 17.

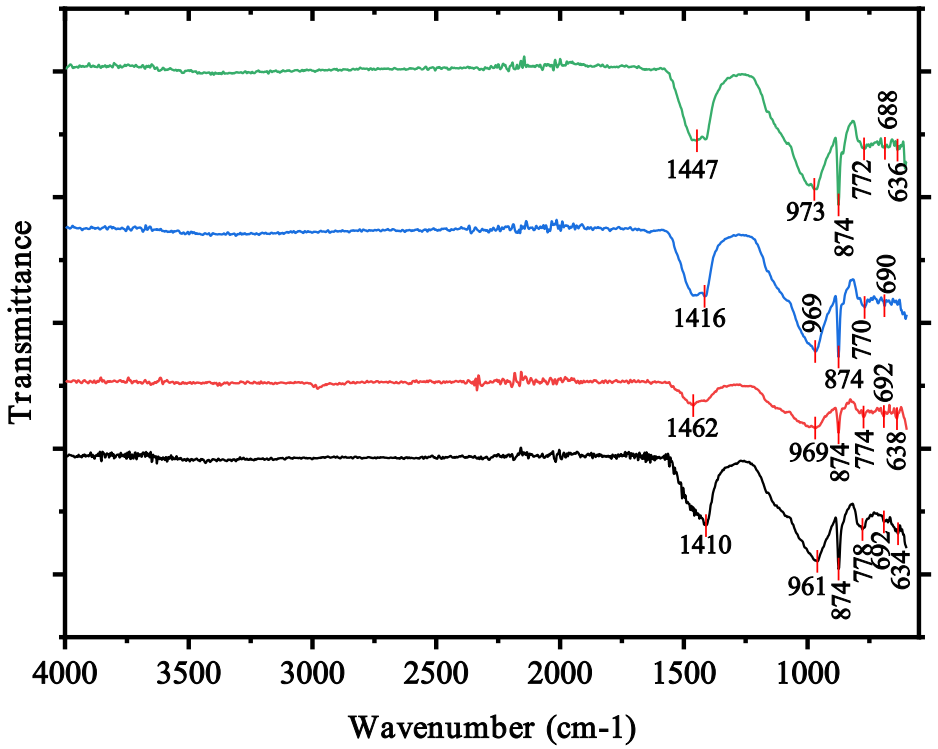

Fig. 17 FTIR spectrum of concrete samples exposed to NaCl for 365 days

FTIR characterization results for NaCl-exposed concrete revealed certain characterization bands at the various wavenumbers. The vibration band at the wavenumbers of 790 cm^{-1} and 852 cm^{-1} is due to an Al-OH bending mode [75]. These peaks were found to be more significant in the case of HVMAC mixes. The Al-OH band at 790 cm^{-1} was found to be negligible for the control sample (C). This vibration band corresponds to the Al-OH stretching vibration of Friedel's salt. This band was found to be higher in the case of HVMAC mixes indicating the increased level of chloride binding owing to the presence of higher aluminate phases in the system. Furthermore, the vibration band at 1490 cm^{-1} is attributed to the C-O bond linking to the presence of carbonate phases that points to the persistence of carbonation, which reduced the constancy of carbonates in AFm phase (monosulfoaluminate). It is for that reason peak was found to be broadened for HVMAC mixes as the existence of Cl^- in the pore solution of concrete replaces CO_3^{2-}/ SO_4^{2-} from monocarbonate/monosulfate phases to form Friedel's salt. Further, an important characteristic band observed at the wavenumber of 961-973 cm^{-1} relates to the Si–O stretching vibrations of C-S-H phase. This peak is more intense for HVMAC mixes,

especially for '20F30G' mix with binder combination of 20% FA+30% GGBFS+50% OPC compared to that of control sample (C). It can be ascribed to the secondary reaction of Pozzolans in the mix to form extra C-S-H phases. The qualitative examination of chloride-attacked concrete samples through FTIR analysis was found to be in agreement with TGA results.

5.2.4 Carbonation test

The change in compressive strength, change in weight and carbonation depth results associated to accelerated carbonation test of all concrete samples cured for both 14 and 28 days are presented in Figs 18-20.

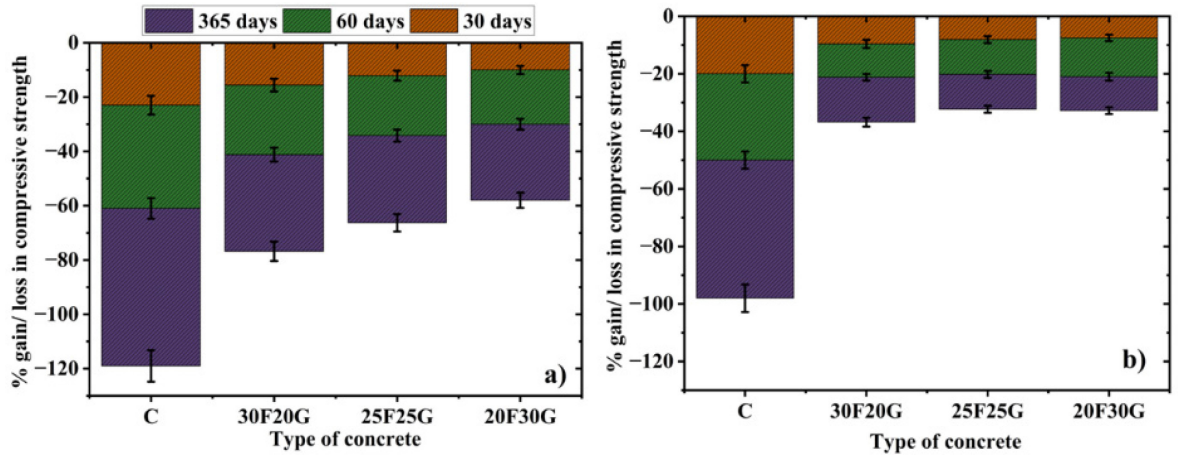

Fig. 18 Compressive strength variation of HVMAC mixes subjected to carbonation environment in a) 14 days and b) 28 days cured concrete samples

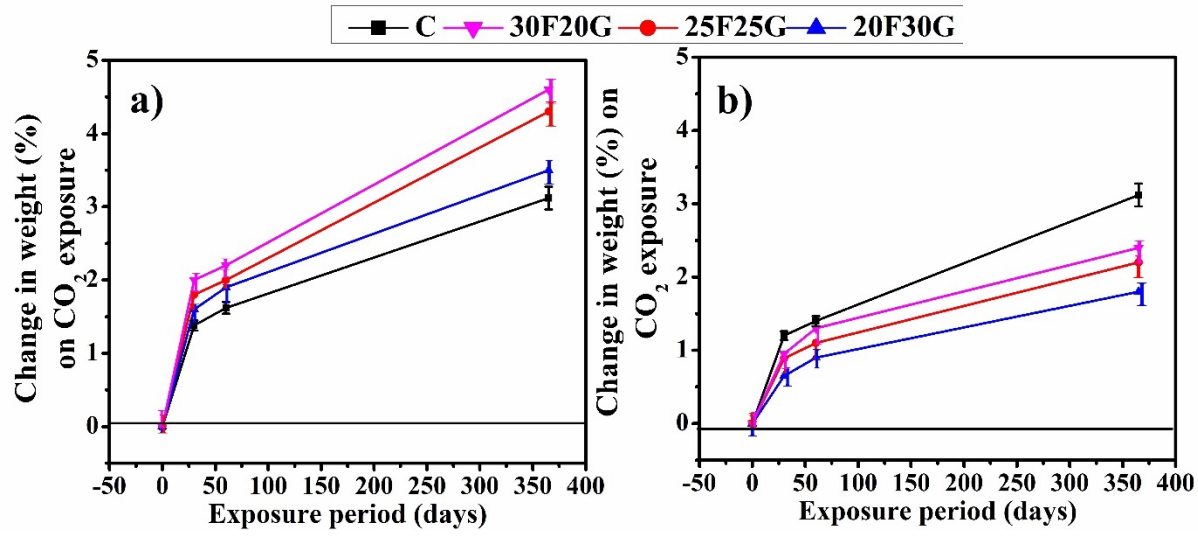

712 **Fig. 19** Change in weight percentage of HVMAC mixes subjected to carbonation in a) 14
713 days cured and b) 28 days cured concrete samples

714 It can be observed from Fig. 18 that compressive strength increased with increasing exposure,
715 irrespective of the type of concrete. However, a significant improvement in compressive
716 strength was noticed up to 60 days exposure, with no significant improvement in strength
717 beyond that. This can be attributed to the beneficial phenomenon of carbonation in densifying
718 the cement matrix leading to the minimized porosity of concrete. This denser structure is
719 associated with the formation of calcite in the pore structure of concrete. Further, it can be
720 noticed from Fig. 18 that among all 14 days cured concrete samples control concrete (C)
721 showed higher compressive strength at all exposure periods compared to that of HVMAC
722 specimens. This is because HVMAC mixes have lower strengths and a huge increase in
723 strength seen upon initial carbonation of these mixes is due to their continued hydration. The
724 increase in strength is much less beyond 30 days of carbonation and this is likely due to reduced
725 portlandite levels. In another case, for 28 days cured concrete samples, certain changes were
726 noticed where 20F30G mix showed closer results to that of control concrete (C). It is the loss
727 of capillary water which accounts for a lot of the strength increase. Indeed, carbonation of C-
728 S-H leads to loss of strength, so the HVMAC mixes will lose strength because of their lower
729 CH contents.

730 All concrete specimens showed an increase in weight with the increase in carbonation duration.
731 This can be attributed to the reduction in pore volume owing to the formation of calcite phase
732 in the pore spaces of concrete. This phenomenon leads to the densified microstructure of
733 concrete thereby resulting in increased weight. This is mainly attributed to the conversion of
734 CH to calcite phase. Control mix without mineral admixture showed higher weight gain at all
735 the curing ages. This can be attributed to the larger formation of stable carbonate phases
736 compared to that of diluted HVMAC mixes as reported in the aforementioned paragraph.
737 However, a slight improvement in weight gain was noticed for 28 days cured HVMAC mixes
738 compared to that of 14 days cured HVMAC mixes. This is because the carbonation resistance
739 of concrete is mainly related to the pore structure and hydration degree as well as carbonating
740 material. Nevertheless, this effect is found to be more proposed in case of mineral admixed
741 concrete compared to that of control concrete (C) owing to the slow reactivity of SCMs.

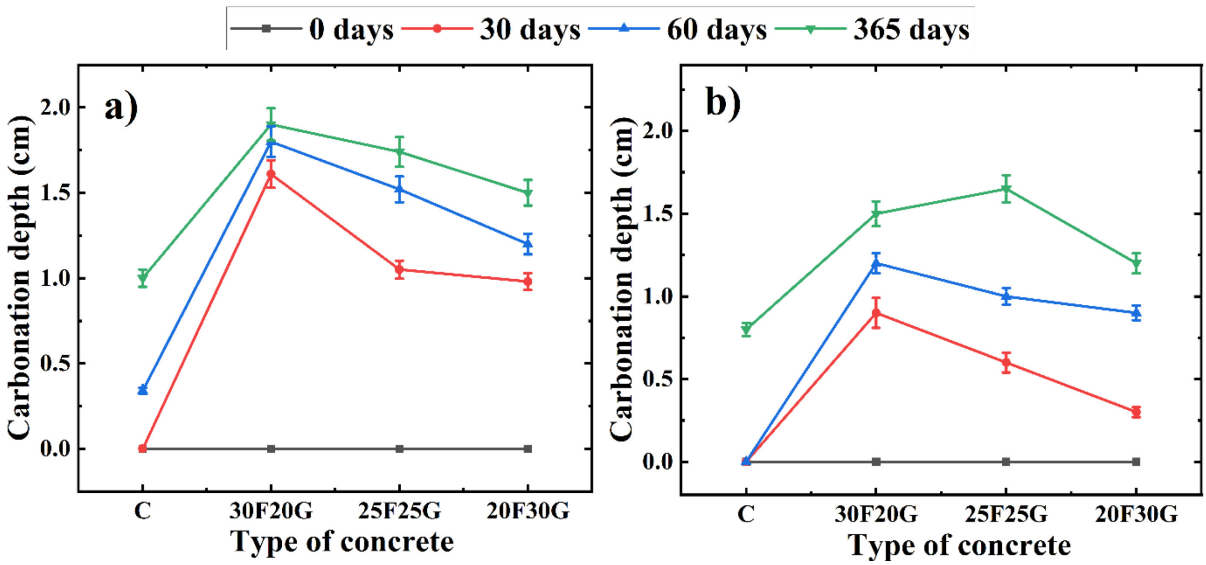

Fig. 20 Carbonation depth in control and HVMAC mixes after exposing to 3.5% CO_2 in a) 14 days cured and b) 28 days cured concrete samples

Carbonation depth refers to the reduction in alkalinity of hydrated cement due to the reaction of carbon dioxide with the alkaline hardened cement paste. The carbonation resistance of concrete depends on the amount of carbonating matter and the permeability, being proportional to the former and inversely proportional to the latter. Figure 20 shows that for both curing durations the control concrete showed the lowest carbonation depth. Dense concrete, prepared with a low w/c ratio can typically show a carbonation depth of 1 cm after 1 year's exposure, while porous and permeable concrete can show carbonation depths ≥5 cm [76]. It should be noted that, even though all HVMAC mixes showed higher carbonation depths than the control concrete, the values fell below 2 cm. So, despite their reduced portlandite contents, pore structure refinement helped to provide a degree of carbonation resistance. Among the HVMAC mixes 20F30G mix showed the least carbonation. This can be ascribed to the densified matrix and the increased reactivity of GGBFS compared to FA.

To assess the phase changes associated with carbonation samples of concrete were collected from a carbonation depth of 1 cm and subjected to thermogravimetric analysis. Fig. 21a) presents the TG-DTG curves of the concrete samples exposed to 365 days of accelerated CO_2.

All DTG traces showed an absence of the endothermic peaks at 400-500 °C attributed to portlandite. Carbonate decomposition is found to start from about 500 °C. This discerns two decomposition stages i) 500-650 °C, and ii) 650-775 °C. This can be attributed to decomposition of poorly crystalline (or amorphous) calcium carbonate phase (vaterite or aragonite) formed from the decalcification of C-S-H for the lower temperature decomposition

765 and decarbonisation of calcite formed from carbonation of portlandite [77]. It is important to
766 note that there is less low-temperature decomposition for the control mix because there is more
767 portlandite, which acts as a buffer preventing C-S-H carbonation. The endothermic peak at the
768 temperature range of 50-200 °C was found to be diminished in the case of carbonated area
769 irrespective of concrete mixes. This indicates the decalcification of calcium ions from the C-
770 S-H and C-A-S-H phases to form polymorphs of calcium carbonate phases. Further, the
771 hydrotalcite phase was also seen for carbonated HVMAC mixes. Based on TGA data,
772 variations in the amount of hydration phases at the carbonation depth of 1 cm for all concrete
773 samples at the exposure period of 365 days were quantified and presented in Fig 21b).

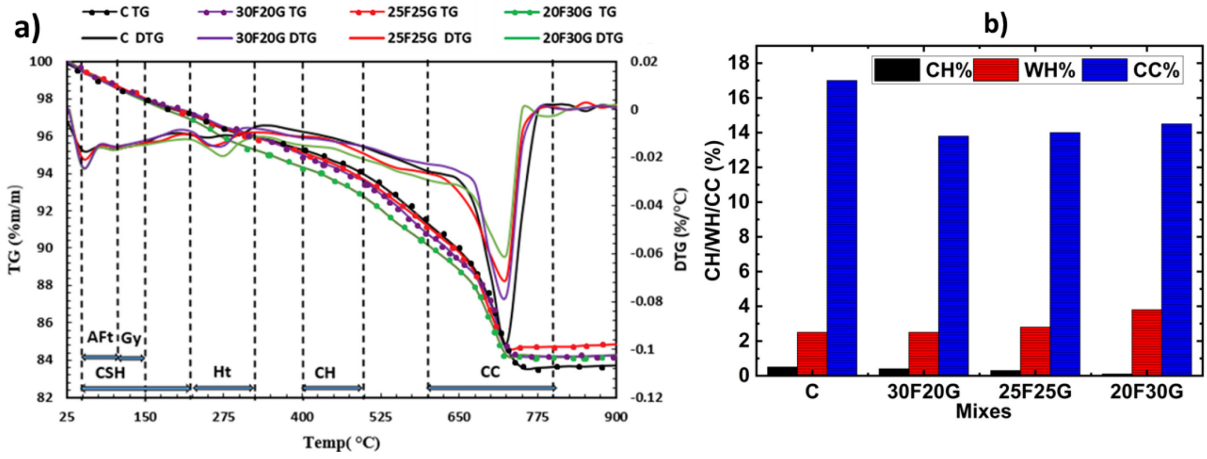

774

775 **Fig. 21 a)** TG-DTG plot for concretes exposed to carbonation environment, **b)** Quantified
776 amount of CH, WH and CC.

777 As anticipated carbonated samples showed the percentage of calcium carbonate than that of
778 non-carbonated samples (ref Fig. 5a)). At the same time, CH and WH contents were seen to be
779 diminished. This is due to the consumption of calcium ions from the hydrated phases caused
780 due to the diffusion of CO_2. An increase in the percentage of CC for concrete samples was
781 found to be in the range of 70-80% to that of non-carbonated samples. The amount of CC for
782 HVMAC mixes was found to be lower due to the occurrence of less CH, the most susceptible
783 phase for carbonation. Further, the dilution effect also influenced the carbonation action.
784 However, calcium-carbonated phases formed in HVMAC mixes can be attributed to the

involvement of C-A-S-H phase in carbonation, which is evidenced by the low carbonate decomposition temperature [78].

Fig. 22 presents the FTIR spectra for carbonated concrete samples exposed to 365 days of accelerated carbonation.

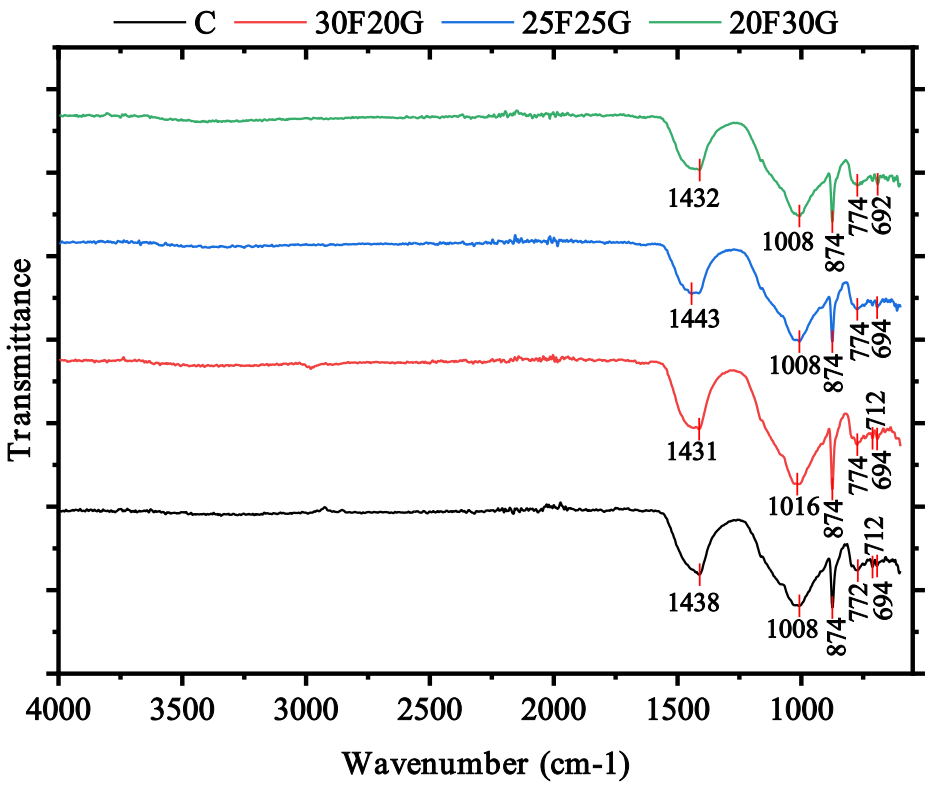

Fig. 22 FTIR spectra of concrete samples exposed to accelerated CO_2 for 365 days

It is well understood that anhydrous calcium carbonate exits in three major polymorphs i.e., calcite, aragonite and vaterite. These polymorphs of $CaCO_3$ can be identified through FTIR spectra due to characteristic vibration bands at specific wavenumbers. Multiple vibration modes are observed in carbonated concrete samples. The asymmetric stretching vibration of CO_3 gives an intensified vibration band at 1431-1443 cm^{-1} that corresponds to the calcite polymorph of calcium carbonate phase. Characteristic peak at the wavenumber of 1008-1016 cm^{-1} corresponds to the stretching of Si–O bond signifying the C-S-H phase has shifted compared to that of non-carbonated specimens. This is because of the decalcification of C-S-H. Characteristic bands at 874 cm^{-1} and 774 cm^{-1} correspond to the out-of-plane bending and in-plane bending mode of carbonates linking to the vaterite polymorphs of calcium carbonate

[79,80]. It is clear from the obtained FTIR spectra formation of calcium carbonate in the calcite polymorph (stable mineral) is more significant in control mix. Whereas, for HVMAC samples intensity of calcite polymorph peaks were seen to be lower than control sample.

6. Conclusions

In general, concrete structures are prone to multiple aggressive environmental actions in India where the conditions are particularly intense along the south-west coast of India. The current study focused on the design and assessment of high-volume mineral admixture concrete (HVMAC) against simulated coastal environmental conditions. However, this study focused on the influence of exposure to single aggressive agents and was coupled with characterization to better understand the reasons behind the durability performance. On this basis, the following conclusions can be made,

1. Mechanical properties such as compressive, split tensile, flexural and bond strength of HVMAC mixes are slightly lower than the corresponding control concrete (C), especially at early ages.
2. Prolonged curing of HVMAC leads to comparable mechanical performance to control concrete (C). From the obtained results, the HVMAC mix '20F30G' achieved higher/comparable strength properties in terms of flexure, tension and bond strength. However, both 25F25G and 20F30G HVMAC mixes have also shown improved compressive strength by the curing age of 56 days.
3. The HVMAC mixes with 50% OPC replacement, performance could be correlated with GGBFS content. Among the HVMAC mixes developed, the concrete mixes with greater GGBFS content showed better performance. This is attributed to the higher reactivity and greater filling ability of GGBS particles in comparison with the fly ash ones. Thus, the synergetic action of multiple mineral admixtures at their optimized proportions with OPC has enhanced the overall performance of concrete.
4. The Sorptivity test results have evidenced the HVMAC concretes reduced susceptibility to capillary suction owing to pore structure refinement arising from the pozzolanic reactions of FA and GGBFS. This development further made the HVMAC mixes less susceptible to deterioration from the action of aggressive ions.
5. The HVMAC with 20% fly ash and 30% GGBFS revealed greater potential in resisting the aggressivity which is further confirmed through TGA and FTIR results.

These results were supported by extensive characterisation of the concretes pre- and post-exposure to various aggressive environments.

1. Thermal analysis of HVMAC hydrated for 28 days displayed an additional endothermic peak at 225-325°C representing the decomposition of hydrotalcite (Ht, $Mg_4Al_2(CO_3)(OH)_{12}.4H_2O$) phase formed due to the existence of MgO delivered by the slag. The presence of mineral admixture significantly reduces the concentration of CH, a primary dissolution phase susceptible to attack by aggressive ions.
2. Examination of hardened concrete systems exposed to acids/sulphates, chlorides and carbon dioxide revealed the existence of detrimental phases such as secondary ettringite (AFt)/secondary gypsum (Gy), Friedel's salt (Fs) and calcite (CC), respectively.
3. In case of both sulphuric acid and magnesium sulphate attack, the transformation of secondary Gy to secondary AFt is found to be less significant. Brucite was formed in concrete exposed to magnesium sulphate solution.
4. TG-DTG analysis illustrated the significant increase in calcium carbonate formation for mixes without mineral admixture (i.e., control concrete (C)). However, in HVMAC, there was evidence of C-S-H decalcification, in addition to portlandite carbonation.

7. Future scope of research

Since the SCMs show their extended influence on the concrete properties at late curing ages, there is a need to study the long-term curing and long-term durability studies on HVMAC. Further, the morphological, mineralogical and various other microstructural studies on HVMAC through advanced characterization techniques may effectively contribute to the scientific community.

Acknowledgement

The authors acknowledge Royal Academy of Engineering, United Kingdom for providing the research grant.

References

[1] Sahoo S, Das BB, Mustakim S. Acid, alkali, and chloride resistance of concrete composed of low-carbonated fly ash. J Mater Civ Eng. 2017;29:4016242. https://doi.org/10.1061/(ASCE)MT.1943-5533.0001759

[2] Sharath BP, Nikunj P, Das BB. Influence of Integration of Iron Ore Tailings on the Physio-mechanical and Microstructure Properties of Fly Ash–Based Coarse Aggregates. J Test Eval. 2023;51:3119–3148. https://doi.org/10.1520/JTE20220466

[3] Mehta A, Siddique R, Ozbakkaloglu T, et al. Fly ash and ground granulated blast furnace slag-based alkali-activated concrete: Mechanical, transport and microstructural properties. Constr Build Mater. 2020;257:119548. https://doi.org/10.1016/j.conbuildmat.2020.119548

[4] Giergiczny Z. Fly ash and slag. Cem Concr Res. 2019;124:105826. https://doi.org/10.1016/j.cemconres.2019.105826

[5] Panda R, Sahoo TK. Effect of replacement of GGBFS and fly ash with cement in concrete. Recent Dev Sustain Infrastruct Sel Proc ICRDSI 2019. Springer; 2021. p. 811–818. https://doi.org/10.1007/978-981-15-4577-1_68

[6] Scrivener KL, John VM, Gartner EM. Eco-efficient cements: Potential economically viable solutions for a low-CO2 cement-based materials industry. Cem Concr Res. 2018;114:2–26. https://doi.org/10.1016/j.cemconres.2018.03.015

[7] Goudar SK, Das BB, Arya SB. Microstructural study of steel-concrete interface and its influence on bond strength of reinforced concrete. Adv Civ Eng Mater. 2019;8. https://doi.org/10.1520/ACEM20180133.

[8] Bellum RR, Muniraj K, Indukuri CSR, et al. Investigation on performance enhancement of fly ash-GGBFS based graphene geopolymer concrete. J Build Eng. 2020;32:101659. https://doi.org/10.1016/j.jobe.2020.101659

[9] Goodarzi F. Characteristics and composition of fly ash from Canadian coal-fired power plants. Fuel. 2006;85:1418–1427. https://doi.org/10.1016/j.fuel.2005.11.022

[10] Li G. Properties of high-volume fly ash concrete incorporating nano-SiO2. Cem Concr Res. 2004;34:1043–1049. https://doi.org/10.1016/j.cemconres.2003.11.013

[11] ASTM C 618. Standard Specification for Coal Fly Ash and Raw or Calcined Natural Pozzolan for Use. Annu B ASTM Stand. 2010;3–6. https://doi.org/10.1520/C0618-15.2.

[12] Das BB, Pandey SP. Influence of fineness of fly ash on the carbonation and electrical conductivity of concrete. J Mater Civ Eng. 2011;23:1365–1368. http://dx.doi.org/10.1061/(ASCE)MT.1943-5533.0000298

[13] Alterary SS, Marei NH. Fly ash properties, characterization, and applications: A review. J King Saud Univ. 2021;33:101536. https://doi.org/10.1016/j.jksus.2021.101536

894 [14] Ahmaruzzaman M. A review on the utilization of fly ash. Prog energy Combust Sci.
895 2010;36:327–363. https://doi.org/10.1016/j.pecs.2009.11.003

896 [15] Rashad AM. A comprehensive overview about the effect of nano-SiO2 on some
897 properties of traditional cementitious materials and alkali-activated fly ash. Constr Build
898 Mater. 2014;52:437–464. https://doi.org/10.1016/j.conbuildmat.2013.10.101

899 [16] Golewski GL, Szostak B. Strengthening the very early-age structure of cementitious
900 composites with coal fly ash via incorporating a novel nanoadmixture based on CSH
901 phase activators. Constr Build Mater. 2021;312:125426.
902 https://doi.org/10.1016/j.conbuildmat.2021.125426

903 [17] Hussain F, Kaur I, Hussain A. Reviewing the influence of GGBFS on concrete
904 properties. Mater Today Proc. 2020;32:997–1004.
905 https://doi.org/10.1016/j.matpr.2020.07.410

906 [18] ASTM C 989. Standard Specification for Slag Cement for Use in Concrete and Mortars.
907 ASTM Stand [Internet]. 2013;44:1–8. https://doi.org/10.1520/C0989.

908 [19] Amran M, Murali G, Khalid NHA, et al. Slag uses in making an ecofriendly and
909 sustainable concrete: A review. Constr Build Mater. 2021;272:121942.
910 https://doi.org/10.1016/j.conbuildmat.2020.121942

911 [20] Goudar SK, Sumukh EP, Das BB. Implication of High-Volume Mineral Admixture on
912 Mechanical Properties and Microstructure At Steel-Concrete Interface. Indian Concr J.
913 2023;97:17–27.

914 [21] Zhou XM, Slater JR, Wavell SE, et al. Effects of PFA and GGBFS on early-ages
915 engineering properties of Portland cement systems. J Adv Concr Technol. 2012;10:74–
916 85. https://doi.org/10.3151/jact.10.74

917 [22] Sumukh EP, Goudar SK, Das BB. Predicting the Service Life of Reinforced Concrete
918 by Incorporating the Experimentally Determined Properties of Steel–Concrete Interface
919 and Corrosion. In: Das BB, Nanukuttan S V, Patnaik AK, et al., editors. Singapore:
920 Springer Singapore; 2021. p. 399–417. Available from:
921 http://link.springer.com/10.1007/978-981-15-8293-6_34. https://doi.org/10.1007/978-
922 981-15-8293-6_34

923 [23] Goudar SK, Sumukh EP, Das BB. Influence Of Marine Environment Exposure On The
924 Engineering Properties Of Steel-concrete Interface. Open Civ Eng J [Internet].

2022;16:1–17. http://dx.doi.org/10.2174/18741495-v16-e221026-2022-HT31-3975-5

[24] Saillio M, Baroghel-Bouny V, Bertin M, et al. Phase assemblage of cement pastes with SCM at different ages. Constr Build Mater. 2019;224:144–157. https://doi.org/10.1016/j.conbuildmat.2019.07.059

[25] Sumukh EP, Goudar SK, Das BB. A Review on the Properties of Steel-Concrete Interface and Characterization Methods. Lect. Notes Civ. Eng. 2021. https://doi.org/10.1007/978-981-15-5001-0_15

[26] Hu Y, Tang Z, Li W, et al. Physical-mechanical properties of fly ash/GGBFS geopolymer composites with recycled aggregates. Constr Build Mater. 2019;226:139–151. https://doi.org/10.1016/j.conbuildmat.2019.07.211

[27] Zhang T, Ma B, Jiang D, et al. Comparative research on the effect of various mineral admixtures on the early hydration process of cement. Constr Build Mater. 2021;301:124372. https://doi.org/10.1016/j.conbuildmat.2021.124372

[28] Zhao H, Hu Y, Tang Z, et al. Deterioration of concrete under coupled aggressive actions associated with load, temperature and chemical attacks: A comprehensive review. Constr Build Mater. 2022;322:126466. https://doi.org/10.1016/j.conbuildmat.2022.126466

[29] Radwan MKH, Onn CC, Mo KH, et al. Sustainable ternary cement blends with high-volume ground granulated blast furnace slag–fly ash. Environ Dev Sustain. 2021;1–35. https://doi.org/10.1007/s10668-021-01633-4

[30] Chen C, Lu C, Lu C, et al. Synergetic effect of fly ash and ground-granulated blast slag on improving the chloride permeability and freeze–thaw resistance of recycled aggregate concrete. Constr Build Mater. 2023;365:130015. https://doi.org/10.1016/j.conbuildmat.2022.130015

[31] IS 12269. Indian Standard ORDINARY PORTLAND CEMENT, 53 GRADE — SPECIFICATION (First Revision). Bur Indian Stand New Delhi. 2013;

[32] BIS 383. Specification for Coarse and Fine Aggregates From Natural Sources for Concrete. Bur. Indian Stand. Delhi. 2016. p. 1–24.

[33] IS:2386 (Part I). Method of test for aggregate for concrete (Particle size and shape). Indian Stand. 1963;(Reaffirmed 2002).

955 [34] Cheah CB, Tiong LL, Ng EP, et al. The engineering performance of concrete containing
956 high volume of ground granulated blast furnace slag and pulverized fly ash with
957 polycarboxylate-based superplasticizer. Constr Build Mater. 2019;202:909–921.
958 https://doi.org/10.1016/j.conbuildmat.2019.01.075

959 [35] IS 516. Method of Tests for Strength of Concrete. Bur Indian Stand. 1959;1–30.

960 [36] IS 5816. Indian standard Splitting tensile strength of concrete- method of test. Bur Indian
961 Stand. 1999;1–14.

962 [37] IS-2770 (Part-I). Methods of Testing Bond in Reinforced Concrete Part 1 pull-out test.
963 Bur Indian Stand New Delhi. 1967;

964 [38] ASTM C1585. Standard Test Method for Measurement of Rate of Absorption of Water
965 by Hydraulic Cement Concretes. ASTM Int. 2013;41:1–6.

966 [39] ASTM C267. Standard Test Methods for Chemical Resistance of Mortars, Grouts, and
967 Monolithic Surfacings and Polymer Concretes. Am Soc Test Mater. 2015;01:1–6.

968 [40] ASTM C1012/C1012M-15. Standard test method for length change of hydraulic-cement
969 mortars exposed to a sulfate solution. ASTM Int West Conshohocken, PA. 2015;11:5–
970 9.

971 [41] AASHTO T-259-02. Resistance of Concrete to Chloride Ion Penetration T 259-02.
972 Aashto [Internet]. 2021;3–5. Available from:
973 https://www.techstreet.com/standards/aashto-t-259-02-2021?product_id=1321045.

974 [42] ISO 1920-12. Testing of concrete-Part 12: Determination of the carbonation resistance
975 of concrete-Accelerated carbonation method(E) ii COPYRIGHT PROTECTED
976 DOCUMENT. 2015;5. Available from: www.iso.orgiTehSTANDARDPREVIEW.

977 [43] Ghods P, Isgor OB, McRae G, et al. The effect of concrete pore solution composition
978 on the quality of passive oxide films on black steel reinforcement. Cem Concr Compos.
979 2009;31:2–11. https://doi.org/10.1016/j.cemconcomp.2008.10.003

980 [44] Recommendations R. CPC-18 Measurement of hardened concrete carbonation depth.
981 Mater Struct. 1988;21:453–455. https://doi.org/10.1007/BF02472327

982 [45] Sumukh EP, Das BB, Barbhuiya S. Effect of Iron Ore and Copper Ore Tailings on
983 Engineering Properties and Hydration Products of Sustainable Cement Mortar. Adv Civ
984 Eng Mater. 2024;13:50–75. https://doi.org/10.1520/ACEM20230031

985 [46] Sumukh EP, Das BB, Barbhuiya S. Synergy of Hydration and Microstructural Properties
986 of Sustainable Cement Mortar Supplemented with Industrial By-Products. Int J Civ Eng.
987 2024;22:1137–1158. https://doi.org/10.1007/s40999-024-00950-9

988 [47] Snehal K, Das BB. Acid, alkali and chloride resistance of binary, ternary and quaternary
989 blended cementitious mortar integrated with nano-silica particles. Cem Concr Compos.
990 2021;123:104214. https://doi.org/10.1016/j.cemconcomp.2021.104214

991 [48] Lothenbach B, Scrivener K, Hooton RD. Supplementary cementitious materials. Cem
992 Concr Res. 2011;41:1244–1256. https://doi.org/10.1016/j.cemconres.2010.12.001

993 [49] Dai J, Wang Q, Xie C, et al. The effect of fineness on the hydration activity index of
994 ground granulated blast furnace slag. Materials (Basel). 2019;12:2984.
995 https://doi.org/10.3390/ma12182984

996 [50] Prince W, Espagne M, Aïtcin P-C. Ettringite formation: A crucial step in cement
997 superplasticizer compatibility. Cem Concr Res. 2003;33:635–641.
998 https://doi.org/10.1016/S0008-8846(02)01042-6

999 [51] Chen W, Huang B, Yuan Y, et al. Deterioration process of concrete exposed to internal
1000 sulfate attack. Materials (Basel). 2020;13:1336. https://doi.org/10.3390/ma13061336

1001 [52] Haha M Ben, Lothenbach B, Le Saout G, et al. Influence of slag chemistry on the
1002 hydration of alkali-activated blast-furnace slag—Part II: Effect of Al2O3. Cem Concr
1003 Res. 2012;42:74–83. https://doi.org/10.1016/j.cemconres.2011.08.005

1004 [53] Kedar HN, Patel S. Effect of hydraulic binders on engineering properties of coal ash for
1005 utilization in pavement layers. Clean Technol Environ Policy. 2024;1–19.
1006 https://doi.org/10.1007/s10098-024-02800-7

1007 [54] Rodriguez ET, Garbev K, Merz D, et al. Thermal stability of CSH phases and
1008 applicability of Richardson and Groves' and Richardson C-(A)-SH (I) models to
1009 synthetic CSH. Cem Concr Res. 2017;93:45–56.
1010 https://doi.org/10.1016/j.cemconres.2016.12.005

1011 [55] Cole WF, Hueber H V. Hydrated magnesium silicates and aluminates formed
1012 synthetically and by the action of seawater on concrete. Silic Ind. 1957;22:75–85.

1013 [56] Ukpata JO, Basheer PAM, Black L. Slag hydration and chloride binding in slag cements
1014 exposed to a combined chloride-sulphate solution. Constr Build Mater. 2019;195:238–
1015 248. https://doi.org/10.1016/j.conbuildmat.2018.11.055

1016 [57] Snehal K, Das BB, Barbhuiya S. Influence of aggressive exposure on the degradation of
1017 nano-silica admixed cementitious mortar integrated with phase change materials. Constr
1018 Build Mater. 2022;335:127467. https://doi.org/10.1016/j.conbuildmat.2022.127467

1019 [58] Snehal K, Das BB, Akanksha M. Early age, hydration, mechanical and microstructure
1020 properties of nano-silica blended cementitious composites. Constr Build Mater.
1021 2020;233:117212. https://doi.org/10.1016/j.conbuildmat.2019.117212

1022 [59] Vaičiukynienė D, Sasnauskas V, Rinkevičius G, et al. Cement hydration with ultrasound
1023 treated clinoptilolite. J Sustain Archit Civ Eng. 2015;11:52–58.
1024 https://doi.org/10.5755/j01.sace.11.2.12430

1025 [60] Mousavi MA, Bahari A. Influence of functionalized MWCNT on microstructure and
1026 mechanical properties of cement paste. Sādhanā. 2019;44:103.
1027 https://doi.org/10.1007/s12046-019-1087-z

1028 [61] Ylmén R, Jäglid U, Steenari B-M, et al. Early hydration and setting of Portland cement
1029 monitored by IR, SEM and Vicat techniques. Cem Concr Res. 2009;39:433–439.
1030 https://doi.org/10.1016/j.cemconres.2009.01.017

1031 [62] Matalkah F, Soroushian P, Balchandra A, et al. Characterization of alkali-activated
1032 nonwood biomass ash–based geopolymer concrete. J Mater Civ Eng.
1033 2017;29:4016270.https://doi.org/10.1061/(ASCE)MT.1943-5533.0001801

1034 [63] Hamilton A, Hall C. Beyond the sorptivity: definition, measurement and properties of
1035 the secondary sorptivity. ASCE J Mater Civ Eng. 2018;30.
1036 https://doi.org/10.1061/(ASCE)MT.1943-5533.0002226

1037 [64] Goudar SK, Das BB, Arya SB. Combined Effect of Marine Environment and pH on the
1038 Impedance of Reinforced Concrete Studied by Electrochemical Impedance
1039 Spectroscopy. Sustain Constr Build Mater. Springer; 2019. p. 635–649.
1040 https://doi.org/10.1007/978-981-13-3317-0_57.

1041 [65] Attiogbe EK, Rizkalla SH. Response of concrete to sulfuric acid attack. ACI Mater J.
1042 1988;85:481–488.

1043 [66] Gutberlet T, Hilbig H, Beddoe RE. Acid attack on hydrated cement—Effect of mineral
1044 acids on the degradation process. Cem Concr Res. 2015;74:35–43.
1045 https://doi.org/10.1016/j.cemconres.2015.03.011

1046 [67] Mollah MYA, Yu W, Schennach R, et al. A Fourier transform infrared spectroscopic

1047 investigation of the early hydration of Portland cement and the influence of sodium
1048 lignosulfonate. Cem Concr Res. 2000;30:267–273. https://doi.org/10.1016/S0008-
1049 8846(99)00243-4

1050 [68] Palacio S, Aitkenhead M, Escudero A, et al. Gypsophile chemistry unveiled: Fourier
1051 transform infrared (FTIR) spectroscopy provides new insight into plant adaptations to
1052 gypsum soils. PLoS One. 2014;9:e107285.
1053 https://doi.org/10.1371/journal.pone.0107285

1054 [69] Habeeb GA, Mahmud HB, Hamid N. Assessment of deterioration in RHA-concrete due
1055 to magnesium sulphate attack. Int J Miner Metall Mater. 2010;17:691–696.
1056 https://doi.org/10.1007/s12613-010-0375-8

1057 [70] Lee S-T. Performance deterioration of Portland cement matrix due to magnesium sulfate
1058 attack. KSCE J Civ Eng. 2007;11:157–163. https://doi.org/10.1007/BF02823896

1059 [71] Polivka M, Brown EH. Influence of various factors on sulfate resistance of concretes
1060 containing pozzolan. Proceedings, Am Soc Test Mats. 1958;58:1077.

1061 [72] Trezza MA, Lavat AE. Analysis of the system 3CaO· Al2O3–CaSO4· 2H2O–CaCO3–
1062 H2O by FT-IR spectroscopy. Cem Concr Res. 2001;31:869–872.
1063 https://doi.org/10.1016/S0008-8846(01)00502-6

1064 [73] Harilal M, George RP, Philip J, et al. Binary blended fly ash concrete with improved
1065 chemical resistance in natural and industrial environments. Environ Sci Pollut Res.
1066 2021;28:28107–28132. https://doi.org/10.1007/s11356-021-12453-4

1067 [74] Glass GK, Buenfeld NR. The influence of chloride binding on the chloride induced
1068 corrosion risk in reinforced concrete. Corros Sci. 2000;42:329–344.
1069 https://doi.org/10.1016/S0010-938X(99)00083-9

1070 [75] Peyvandi A, Holmes D, Balachandra AM, et al. Quantitative analysis of chloride ion
1071 diffusion in cementitious materials using Al 27 NMR spectroscopy. J Infrastruct Syst.
1072 2015;21:4014047. https://doi.org/10.1061/(ASCE)IS.1943-555X.0000236

1073 [76] Rodriguez-Navarro C, Kudłacz K, Cizer Ö, et al. Formation of amorphous calcium
1074 carbonate and its transformation into mesostructured calcite. CrystEngComm.
1075 2015;17:58–72. https://doi.org/10.1039/C4CE01562B

1076 [77] Herterich JA, Black L, Richardson I. Microstructure and phase assemblage of low-
1077 clinker cements during early stages of carbonation. 14th Int Congr Chem Cem (ICCC

2015) Abstr B Vol 1. Leeds; 2015. http://eprints.whiterose.ac.uk/96988/

[78] Chen Z, Lee Y, Cho H, et al. Improvement in Carbonation Resistance of Portland Cement Mortar Incorporating γ-Dicalcium Silicate. Adv Mater Sci Eng. 2019;2019:9856734. https://doi.org/10.1155/2019/9856734

[79] Herterich J, Richardson I, Moro F, et al. Microstructure and phase assemblage of low-clinker cements during the early stages of carbonation. Cem Concr Res. 2022;152:106643. https://doi.org/10.1016/j.cemconres.2021.106643

[80] Myszka B, Schüßler M, Hurle K, et al. Phase-specific bioactivity and altered Ostwald ripening pathways of calcium carbonate polymorphs in simulated body fluid. RSC Adv. 2019;9:18232–18244. https://doi.org/10.1039/C9RA01473J